

ARTICLE

Brain-infiltrating ILC2s boost poststroke angiogenic initiation through α -CGRP production

An Ping^{1,2,4}*, Fan Yang^{1,2}*, Lingxiao Lu^{1,2}, Xiaotao Zhang^{1,2}, Jianan Lu^{1,2}, Huaming Li^{1,2}, Yichen Gu^{1,2}, Ziyang Jin^{1,2}, Jianmin Zhang^{1,2,3}, and Ligen Shi^{1,2,3}

Group 2 innate lymphoid cells (ILC2s) regulate immunity and tissue repair but are rarely found in the brain. Whether ILC2s can infiltrate the brain from bloodstream and the underlying mechanisms involved remain unclear. While ILC2s have recently been identified as key immunosuppressive players in neuroinflammation, their role in brain tissue repair remains promising but underexplored. Here, using *in vivo* and *in vitro* expansion of ILC2s, we demonstrate that ILC2s can enter the brain parenchyma from the blood circulation early after ischemic stroke in a CXCR1-dependent manner. Once in the brain, ILC2s improve long-term recovery of sensory-motor functions by promoting initiation of angiogenesis, namely angiogenic sprouting. Mechanistically, ILC2s produce α -calcitonin gene-related peptide (α -CGRP) to enhance angiogenic sprouting. ILC2s depleted of α -CGRP infiltrate the brain but fail to initiate angiogenesis. Impaired function of CGRP receptors on cerebrovascular endothelial cells abolishes the angiogenic effect of ILC2s. These findings highlight ILC2s as a promising target for promoting therapeutic angiogenesis in stroke recovery.

Introduction

As an integral component of the innate immune system, innate lymphoid cells (ILCs) and their precursor cells circulate along the blood stream during embryonic development but are scarcely seen in the blood circulation after birth (Ghaedi et al., 2016; Hernández-Torres and Stehle, 2022; Ikawa et al., 2004). In adults, ILCs primarily reside in barrier tissues such as the lung and intestine (Mamuladze and Kipnis, 2023; Wang and van de Pavert, 2022). Among ILCs, group 1 ILC (ILC1) and group 3 ILC (ILC3) are mainly associated with pro-inflammatory responses and antigen presentation, whereas group 2 ILC (ILC2) is characterized by its role in immune regulation, tissue protection, and tissue repair (Ghaedi and Takei, 2021; Vivier et al., 2018). ILC2s have been shown to promote homeostasis and repair of respiratory epithelium (Monticelli et al., 2011), intestinal mucosa (Cho et al., 2019), and renal tubules (Cao et al., 2018) following acute respiratory injury, acute colitis, and acute kidney injury. The protective role of ILC2s in peripheral tissues suggest that it might also play a similarly important role in the recovery of brain injury.

ILC2s are rarely seen in the brain of healthy adults. It is known that ILC2 and their precursor cells possess the ability to migrate into organs through blood circulation during embryonic development (Bando et al., 2015; Schneider et al., 2019) or inflammation of peripheral organs (Bartemes et al., 2014; Stier

et al., 2018). Following brain injury, the brain upregulates chemokines, enabling immune cells to enter the brain via the bloodstream (Shi et al., 2019). However, the number of ILC2s in the peripheral circulation is extremely low, comprising only 0.05% of peripheral blood mononuclear cells in adults (Xing et al., 2017), with an even lower proportion in mice (Jackson et al., 2014). This scarcity may result in an insufficient replenishment of ILC2s from the blood, making it hard to maintain a stable population within the brain parenchyma after injury. Additionally, the functioning blood-brain barrier (BBB) in adults can limit the infiltration of immune cells, which may block the access of ILC2s to the brain. The questions remain that whether ILC2s can infiltrate the brain from blood, and the mechanisms underlying such infiltration require further investigation.

Despite of the limited number of ILC2s in the blood and brain, recent studies have found that *in vivo* expansion of ILC2s can exert immunosuppressive effects during acute and chronic neuroinflammation in the central nervous system (Fung et al., 2020; Gadani et al., 2017; Liu et al., 2024; Zheng et al., 2023). ILC2s can be expanded *in vivo* by either IL 33 (IL-33) (Fung et al., 2020; Gadani et al., 2017; Liu et al., 2024; Zheng et al., 2023) or IL2/IL2Ab complex (IL2–JES6-1) (Engelbertsen et al., 2015; Newland et al., 2017; Yu et al., 2021). IL-33 exerts its biological

^{© 2025} Ping et al. This article is distributed under the terms as described at https://rupress.org/pages/terms102024/.



¹Department of Neurosurgery, Second Affiliated Hospital, School of Medicine, Zhejiang University, Hangzhou, China; ²Clinical Research Center for Neurological Diseases of Zhejiang Province, Hangzhou, China; ³Binjiang Institute of Zhejiang University, Hangzhou, China; ⁴State Key Laboratory of Transvascular Implantation Devices, Hangzhou, China; ⁵China

^{*}A. Ping and F. Yang contributed equally to this paper. Correspondence to Ligen Shi: slg0904@zju.edu.cn; Jianmin Zhang: zjm135@zju.edu.cn.



effects by binding to ST2 expressed on the surface of ILC2s and T cells. IL2-JES6-1 selectively targets the alpha subunit of the IL-2 receptor present on ILC2s and regulatory T cells (Tregs). The expansion of ILC2s has been shown to mitigate neuroinflammation during the acute phase following cerebrovascular disease through cytokines such as IL-4 (Zheng et al., 2023) and IL-13 (Liu et al., 2024). Activated meningeal ILC2s secrete IL-13 and IL-5, thereby reducing neuroinflammation following spinal cord injury (Gadani et al., 2017). In aged mice, expansion of choroid plexus ILC2s secrete IL-5, which suppress chronic neuroinflammation and improve cognitive function (Fung et al., 2020). These studies focus on mitigating neuroinflammation of the brain and spinal cord, highlighting the role of ILC2s in suppressing neuroinflammation and modulating immune responses. However, whether ILC2s can promote tissue repair following brain injury remains underexplored.

ILC2s exhibit a strong tissue repair capacity in peripheral tissues. Their reparative effects are closely linked to the vascular system: ILC2s have been shown to promote cardiac repair following myocardial ischemia, to reduce collagen content in scar tissue, and to improve the quality of tissue remodeling (Yu et al., 2021). In the formation of atherosclerotic plaques, ILC2s can indirectly promote vascular healing of the arterial intima by modulating the phenotype of macrophages within the plaques (Newland et al., 2017). Additionally, ILC2s have been proven to protect endothelial cells, reducing pyroptosis in lung endothelial cells during sepsis (Lai et al., 2018). However, whether ILC2s exhibit similar reparative potential in the brain remains unexplored. Angiogenesis is a crucial step in tissue repair following cerebral infarction, contributing to reperfusion and the formation of collateral circulation. Therefore, the pro-angiogenic capacity of ILC2s could be crucial for brain repair. Recent studies indicate that poststroke vascular neogenesis primarily occurs through sprouting, where blood vessels in the ischemic area undergo stages of sprouting, tubulogenesis, and maturation to form fully functioning new blood vessels. Previous studies on poststroke vascular neogenesis have been largely focused on the outcomes (pro-angiogenic/antiangiogenic) rather than the specific stages of the angiogenic process, limiting the potential for targeted provascular therapy by modulating specific stages. ILC2s' involvement in interaction with the vascular system and endothelial cells suggests the possible involvement of ILC2s in certain stages of brain vascular repair as well.

In the present study, we systemically evaluated the long-term therapeutic effects of IL2–JES6-1 in a murine model of ischemic stroke. By single-cell RNA sequencing (scRNA-seq) analysis of infiltrating immune cells 14 days after stroke, we unexpectedly discovered ILC2s as the most prominently expanded lymphocytes among the brain-infiltrating immune cells after IL2–JES6-1 treatment. Subsequent analysis revealed that circulating ILC2s infiltrate during the subacute phases after ischemic stroke and mediate functional recovery. Furthermore, our results demonstrated the unique role of the brain-infiltrating ILC2s in post-stroke tissue repair via α -calcitonin gene-related peptide (α -CGRP)-mediated angiogenic sprouting of vascular endothelial cells. Taken together, our findings illustrate functional characteristics of circulating ILC2s in brain-infiltration and

promoting angiogenic sprouting, opening up possibilities for cell-based immune therapy for therapeutic angiogenesis after ischemic stroke.

Results

ILC2s accumulate in the brain following ischemic stroke and possess potential tissue reparative phenotype

We performed scRNA-seq of brain-infiltrating immune cells (CD45high) 14 days after intermittent administration of the IL2-JES6-1 complex (seven injections, from 6 h to 14 days after the surgery) in transient middle cerebral artery occlusion (MCAO) models (Fig. 1, A and B). 18,760 cells from two animals in the IL2– JES6-1-treated group (with 17,076 cells passing quality control, n = 2) and 25,482 cells from two animals in the PBS control group (MCAO mice receiving intraperitoneal PBS injection after surgery, with 23,714 cells passing quality control, n = 2). scRNA-seq revealed a significantly expanded cell population within the brain-infiltrating immune cells following IL2-JES6-1 treatment (Fig. 1 C). These cells exhibited upregulated expression of canonical ILC2s marker genes, including Gata3, IlIrl1, Klrq1, Il17rb, Il7r, and Icos, suggesting their identity as ILC2s (Fig. S1). The high expression of Il2ra in these cells suggested their robust responsiveness to the IL2-JES6-1 complex. Furthermore, the absence of Trac expression distinguished them from type 2 helper T cells (Fig. S1). In accordance to scRNA-seq results, CD45+CD3-GATA3+ ILC2s were observed within the ischemic core 14 days after MCAO and IL2-JES6-1 treatment (Fig. 1 D). Next, we performed flow cytometry analysis on immune cells isolated from the ischemic hemispheres of the mice treated with IL2-JES6-1 14 days after MCAO (Fig. 1 E). We found the ratio of ILC2s (CD45+Lin-ST2+KLRG1+CD127+ cells) over CD45high cells expanded from around 0.2-2% by IL2-JES6-1 treatment. Thus, results from scRNA-seq and flow cytometry agree that IL2-JES6-1 complex can intrinsically expand ILC2s number by around 10 times after MCAO.

To examine the tissue-reparative potential of ILC2s and other brain immune cells, we calculated the AUCell score (Aibar et al., 2017) of the tissue reparative gene set (Arg1 [Campbell et al., 2013], Areg [Zaiss et al., 2015], Il4 [Zheng et al., 2023], Il5 [Leitch et al., 2009], Il13 [Allen, 2023], Tafb1 [Deng et al., 2024], Csf2 [Hinks et al., 2019], Spp1 [Shi et al., 2021], and Vegfa [Hayakawa et al., 2011]) (Fig. 1 F). The result indicated the tissuereparative potential of ILC2s compared with other immune cells. To further resolve the functional characteristics of ILC2s, we performed GOBP analysis to the differentially expressed genes (DEGs) in ILC2s (Fig. 1 G). Among top 50 significant terms, most terms are related to immune regulation (26 terms), since type 2 regulatory function is a major effect of ILC2s (Mamuladze and Kipnis, 2023). The remaining terms can be classified as tissue remodeling functions (12 terms, shown in the lower part of Fig. 1 G) and metabolic functions (12 terms).

To validate the potential reparative effect of ILC2s on subacute and long-term outcomes poststroke, we extracted ILC2s from bone marrow and spleen of donor mice and transferred them to MCAO mice after *in vivo* expansion and strict purification (Fig. 1 H). We followed a classical ILC2 expansion protocol



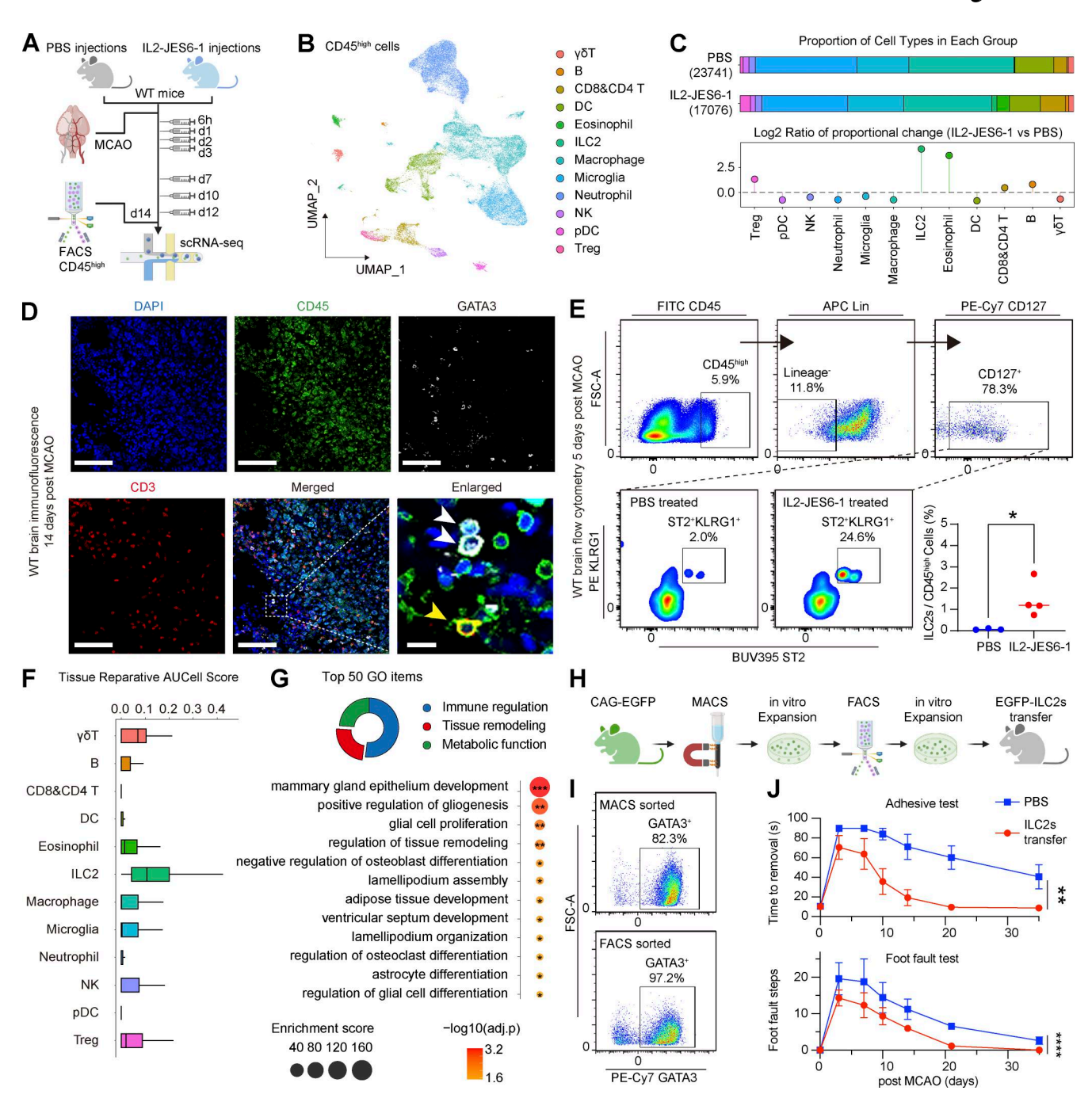


Figure 1. Accumulating brain ILC2s possess potential pro-tissue repair functions following ischemic stroke. (A) Experimental design for scRNA-seq of CD45^{high} immune cells (created with https://BioRender.com). n = 2 biological replicates for each group. (B) UMAP plot of CD45^{high} immune cells with (n = 2) and without (n = 2) IL2–JES6-1 treatment 14 days after MCAO. (C) The relative proportion (upper row) of all cell types in A from each group and proportional change (lower row) of these cell types between IL2–JES6-1-treated group and PBS group. (D) Immunofluorescence of a WT mouse brain 14 days after MCAO receiving IL2–JES6-1 treatments. The white arrows indicate ILC2s (CD45+CD3-GATA3+), and yellow arrow indicates a T cell (CD45+CD3+). Scale bars, 100 μ m (10 μ m for zoomed out). (E) Flow cytometry gating strategy and quantification of ILC2s/CD45^{high} cells ratio 14 days after MCAO, with (24.6%, 54 cells) or without (2.0%, 9 cells) IL2–JES6-1 treatment (n = 3 for PBS group, n = 4 for IL2–JES6-1-treated group), analyzed by two-sided, unpaired Student's t = 1 test. All data represent biological replicates from two independent experiments. *P = 0.0397. (F) A comparison of tissue reparative potential of each cell type evaluated by AUCell. NK, nature killer cell; DC, dendritic cell; pDC, plasmacytoid dendritic cell. (G) Reactome pathway enrichment results of DEGs of ILC2s, compared with other CD45^{high} immune cells. The pie chart above indicates the total hits of DEGs involved in Reactome terms. The lower bubble plot shows 10 top pathways enriched. (H) Experimental design for ILC2s extraction, purification, transferring, and tracing (created with https://BioRender.com). (I) Flow cytometry results showing purity of ILC2s after MACS and FACS. (J) Behavioral tests of MCAO mice after PBS treatment and ILC2s transfer (n = 8), analyzed by two-way ANOVA repeated measurement. Data are shown as line charts with error bars (SEM, median). **P = 0.0034; *****P < 0.0001.



(Puttur et al., 2019), first amplified ILC2s in vivo in EGFP mice by IL-33 injections for a week, followed by MACS sorting of Lin-CD25⁺ cells from bone marrow and spleen (Fig. 1 I, upper). After in vitro culture and expansion for 2 wk, we performed FACS sorting of CD45+Lin-ST2+KLRG1+CD127+ cells (Fig. 1 I, lower) using the same strategy as in Fig. 1 E. We then used an in vitro expansion method developed by Li et al. (2024). After 4 wk of expansion, ILC2s were harvested for further experiments. ILC2s were intravenously transferred 6 h after MCAO, and their sensory-motor function was evaluated afterward at days 3, 7, 10, 14, 21, and 35. We assessed the time required for removing adhesive substances from the contralateral forelimb (Fig. 1 J, upper) and the number of foot faults while walking on a grid (Fig. 1 J, lower). The results revealed differences in sensorymotor function (adhesive test) beginning at day 10; from day 21 onward, mice treated with ILC2s demonstrated significantly better sensory-motor function compared with the control group. These findings showed that exogenous ILC2s play a crucial role in functional recovery after ischemic stroke.

ILC2s enter the brain from peripheral circulation in a CXCR1dependent manner

In adults, ILC2s generally resides within bone marrow and peripheral tissues (lung, small intestine, etc.) and can traffic via hematogenous migration (Puttur et al., 2019; Ricardo-Gonzalez et al., 2018; Stier et al., 2018); we investigate whether ILC2s in the peripheral circulation during the acute phase could infiltrate the brain parenchyma. Through i.v. transfer of EGFP-ILC2s (Fig. 1, H and I), we were able to track circulating ILC2s and their infiltration into the brain after MCAO (Fig. 2 A): 6 h after the MCAO modeling, 1×10^6 EGFP-ILC2s were i.v. transferred into the mice. The number and distribution of EGFP-positive cells in the brain were observed at multiple time points (days 1, 3, 5, 10, and 14) after MCAO (Fig. 2 B). EGFP-positive cells appeared in the thalamus on day 3 and were widely distributed in the thalamus, basal ganglia, and cortex by day 5 (Fig. 2, B and C). Nearly all EGFP-positive cells located in the ischemic hemisphere. By day 7, a large amount of ILC2 still widely existed in brain, but the total number ceased to increase. By day 14, they were undetectable in the thalamus and basal ganglia, with cortical areas unidentifiable due to tissue dehydration during immunostaining (Fig. 2 B). We also performed flow cytometry to monitor the proportional change of ILC2s in the blood and brain at days 5 and 14 after MCAO (Fig. S2). The results also showed higher proportion of ILC2s at day 5 after MCAO (Fig. S2, A and C), especially in the ischemic brain (Fig. S2 C). Lower proportion of ILC2s were observed at day 14 after MCAO (Fig. S2, B and D).

Next, we explored the mechanism underlying the infiltration. To compare the transcriptional profiles of ILC2s at key time points, we collected the transferred EGFP-ILC2s from the blood at day 1 (blood 1d, n=6) and day 5 (blood 5d, n=6), also from the brain at day 5 after MCAO (brain 5d, n=6) for RNA sequencing-based switching mechanism at 5' end of the RNA transcript (SMART-seq) (Fig. 2 A). In addition, ILC2s directly from culture medium (base, n=5) were also included as a baseline control. To compare functional difference between groups, we performed Gene Set Variation Analysis using curated gene sets (Agrawal

et al., 2023; Milacic et al., 2023) based on the normalized expression matrix (Fig. 2 E), as well as Kyoto Encyclopedia of Genes and Genomes enrichment analysis based on top DEGs (adjusted P < 0.05, Fig. S3, A-C). Gene Set Variation Analysis and Kyoto Encyclopedia of Genes and Genomes terms related to immune responses and cell activation were enriched (Fig. 2 E and Fig. S3 A) after ILC2s entered blood circulation. From day 1 to 5, ILC2s in the blood kept receiving signals for activation and differentiation (Fig. 2 E and Fig. S3 B), indicating potential adaptation to blood environment. Upon entering the brain (Fig. 2 E, brain 5d versus blood 5d), ILC2s acquired adhesive phenotype and tissue-remodeling functions (Fig. 2 E and Fig. S3 C, for overall changes across four groups, see Fig. S3, D-F).

To further distinguish the key effectors in blood-brain migration of ILC2s, we search for chemokine receptors and in DEGs between blood ILC2s at days 5 and 1 (Fig. 2 F). The result showed ILC2s had a marked increase of *Cxcr1* at mRNA level. Using flow cytometry, we compared the expression of CXCR1 on transferred ILC2s at days 1 and 5 after MCAO (Fig. 2 G), which showed ILC2s at day 5 express higher level of CXCR1 (Fig. 2 H). SCH563705, a noncompetitive antagonist of CXCR1 was added to the culture medium for blockage of CXCR1 on ILC2s (Fig. 2 I). Incubated ILC2s were transferred after MCAO as described above. The infiltration of ILC2s was compromised after incubated with SCH563705 (Fig. 2, J and K). Taken together, these findings demonstrate that ILC2s upregulate functions related to cell-cell signaling and enter the brain through a CXCR1-dependent way.

Transferred ILC2s promote angiogenesis and vascular development after ischemic stroke

Long-term functional recovery after ischemic stroke could result from improvements of various components of the brain, including the neurovascular unit collaboration and white matter integrity. To investigate the key mechanism of ILC2-mediated long-term recovery, we performed scRNA-seq of the infarcted hemisphere at day 14 after MCAO (Fig. 3 A). The structural components, including astrocytes, pericytes, and endothelial cells, as well as myelin-associated cells, including oligodendrocytes and oligodendrocyte precursor cells, are included into the following analysis (Fig. 3 B). Between ILC2-transferred group and PBS group, the count of upregulated DEGs, cell proportional ratio, and AUCell score for wound healing (Gene Ontology [GO]: 0042060) were calculated for each type of cells. The results highlight endothelial cells as a top beneficiary from ILC2s treatment, ranking second in upregulated genes, fifth in increased cell proportion ratio, and second in AUCell score for healing. These results suggest that ILC2s may have a favorable effect on the vascular endothelial remodeling in the chronic phase after MCAO, particularly by positively regulating endothelial cells in terms of both quantity and function.

Following ischemia-reperfusion injury poststroke, impaired vascular viability, integrity, and BBB disruption often occur in the infarct core and penumbra regions (Shi et al., 2016), leading to compromised exchange of substance and exacerbated infiltration of peripheral immune cells, which aggravate neuro-inflammation and impair the process of neural functional recovery (Shi et al., 2021). Therefore, poststroke vascular



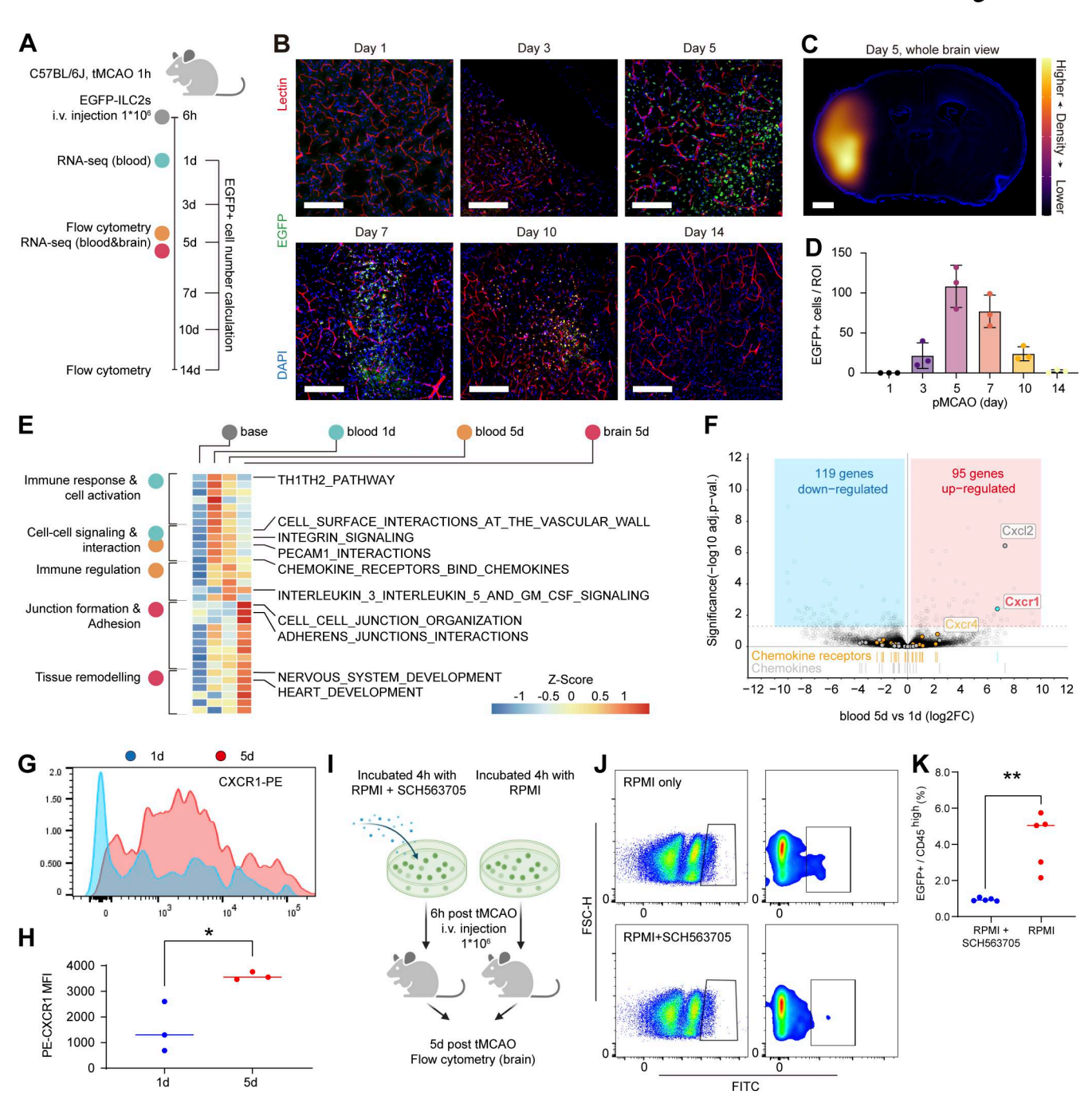


Figure 2. **ILC2s enter the brain from peripheral circulation in a CXCR1-dependent manner. (A)** Experimental design of tracing and RNA sequencing of transferred EGFP-ILC2s *in vivo* (created with https://BioRender.com). **(B)** Changes in EGFP-positive cells in ischemic areas at different time points after MCAO modeling and EGFP-ILC2s transfer. Scale bars, 200 μm. **(C)** Density map showing brain-wide distribution of EGFP-positive cells 5 days after MCAO. Brighter color indicates higher density. Scale bar, 500 μm. **(D)** EGFP-positive cell counts per view from day 1 to 14 (*n* = 3). **(E)** Heatmap showing averaged and normalized GSVA results of four groups of ILC2s. **(F)** Volcano plot of DEGs of ILC2s between groups (|log2FC| > 0.25, adjusted P < 0.05). **(G and H)** Quantification of CXCR1 expression on brain-infiltrating ILC2s at day 1 and 5 after MCAO and EGFP-ILC2s transfer (*n* = 3), analyzed by two-sided, unpaired Student's *t* test. All data represent biological replicates from two independent experiments. *P = 0.0226. **(I)** ILC2s were cultured in the presence of SCH563705+RPMI or RPMI only for 6 h before transferring (created with https://BioRender.com). **(J and K)** Flow cytometry gating strategy and quantification of transferred ILC2s at day 5 after ischemic stroke (*n* = 5), analyzed by two-sided, unpaired Student's *t* test. All data represent biological replicates from two independent experiments. **P = 0.0015. GSVA, Gene Set Variation Analysis.

neogenesis and maturation are considered beneficial for neural functional recovery.

We validate the endothelial changes using immunofluorescence. By intravenously injecting Evans blue at poststroke day 14

and evaluating the proportion of intracerebral leakage area in the basal ganglia region, we found that the BBB in the ILC2transferred group maintained better barrier function, with a significantly smaller leakage area proportion than the sham



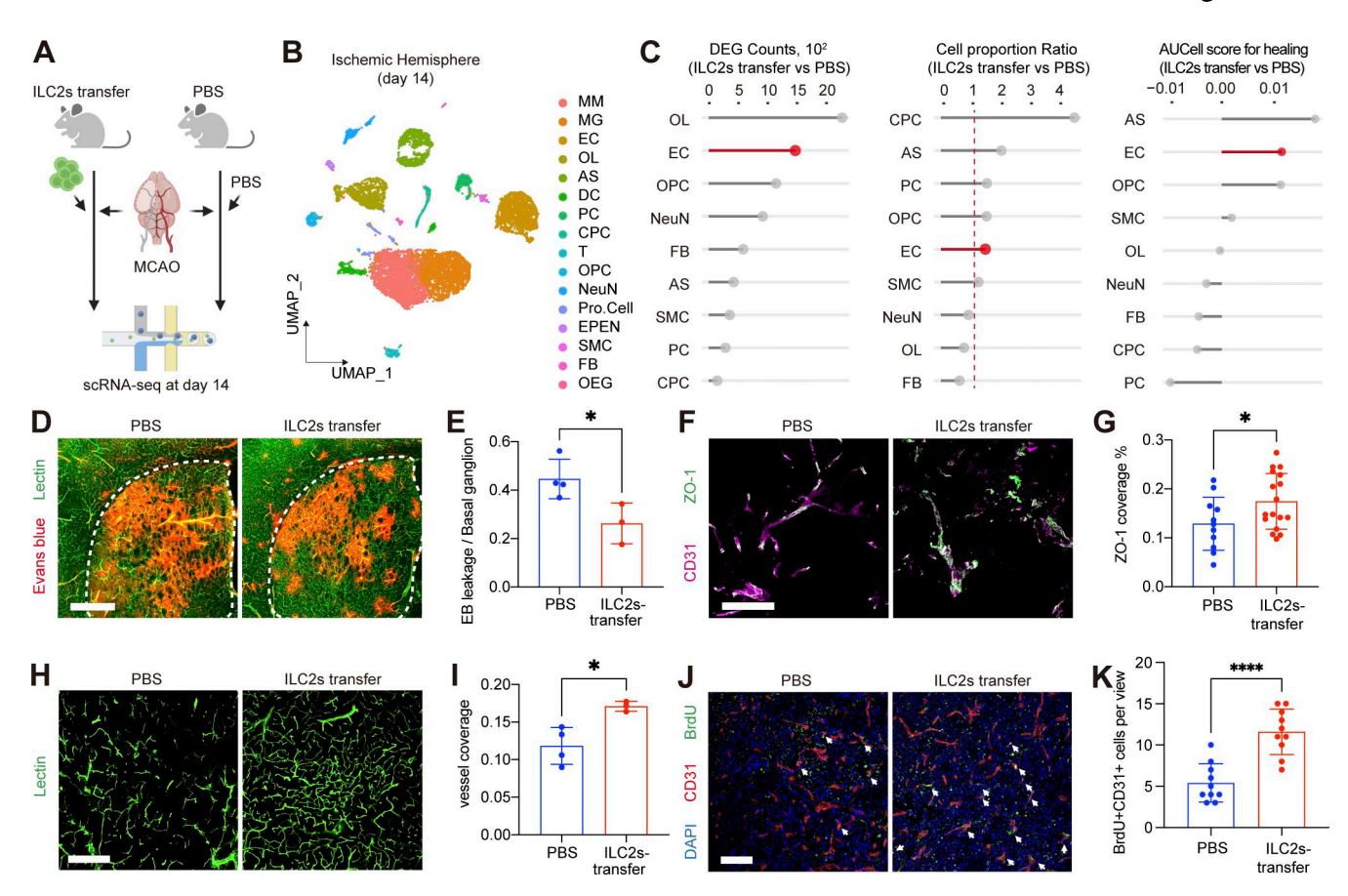


Figure 3. Transferred ILC2s promote angiogenesis and vascular development after ischemic stroke. (A) Experimental design of scRNA-seq of ischemic hemisphere after MCAO and ILC2s transfer (created with https://BioRender.com). (B) UMAP plot of scRNA-seq clustering at 14 days poststroke in the ischemic hemisphere with and without i.v. transfer of ILC2s. MM, monocyte and macrophage; MG, microglia; EC, endothelial cell; OL, oligodendrocyte; AS, astrocytes; DC, dendritic cell; PC, pericyte; CPC, choroid plexus cells; T, T cells; OPC, oligodendrocyte precursor cell; NeuN, neuron; Pro.Cell, proliferating cell; EPEN, ependymal cells; SMC, smooth muscle cell; FB, fibroblast; OEG, olfactory ensheathing glia. (C) Number of DEGs in different cell types (left column), ratio of cell proportion (middle column), and AUCell score for healing (right column), ILC2-transferred group versus PBS group. (D and E) Lectin and Evans blue staining results and the quantification at 14 days after stroke in PBS group (n = 4) and ILC2-transfer group (n = 3). White dashed lines indicate basal ganglion area. The bar plot was analyzed by two-sided, unpaired Student's t test. All data represent biological replicates from two independent experiments. *P = 0.0334. Scale bar, 500 µm. (F and G) Immunofluorescence of ZO-1 and CD31 staining and ZO-1 coverage quantification at day 14 after stroke (n = 3, 12 views for each group, each dot stands for a view). The bar plot was analyzed by two-sided, unpaired Student's t test. All data represent biological replicates from two independent experiments. *P = 0.0449. Scale bar, 100 μ m. (H and I) Immunofluorescence of lectin-488 staining and quantification for vessel coverage in PBS group (n = 4) and ILC2-transfer group (n = 3) within the basal ganglia region at day 14 after MCAO. The bar plot was analyzed by two-sided, unpaired Student's t test. All data represent biological replicates from two independent experiments. *P = 0.0166. Scale bar, 200 μm. (J and K) Immunofluorescence of BrdU and CD31 and quantification of BrdU+CD31+ cell proportion in the basal ganglia region the staining results at 14 days after stroke in the two groups (n = 3, 10 views for each group, each dot stands for a view). The bar plot was analyzed by two-sided, unpaired Student's t test. All data represent biological replicates from two independent experiments. ****P < 0.0001. Scale bar, 100 µm. ZO-1, tight junction-associated proteins.

group (Fig. 3, C and D). Evaluation of tight junction-associated proteins coverage among endothelial cells similarly showed more complete inter-endothelial tight junctions in the ILC2-transferred group (Fig. 3, E and F). Thus, ILC2-transferred group surpass PBS group on integrity of brain vascular network, possessing improved endothelial-endothelial integrity.

To determine whether ILC2s facilitate poststroke beneficial remodeling of blood vessels, we quantified the number of functioning blood vessels and assessed tight junctions of blood vessels 14 days after stroke. Lectin (DyLight 488) was used to label functioning vessels. In the infarct area, the lectin+ vessel coverage in the ILC2-transferred group was ~10% higher than that in the sham group (Fig. 3, G and H). To quantify endothelial neogenesis, we injected BrdU daily from day 4 to 10 (Williamson

et al., 2021) after stroke and counted the number of BrdU+CD31⁺ cells at day 14 (Fig. 3, I and J). In the infarct area, the number of newly generated endothelial cells was significantly higher in the ILC2-transferred group than in the sham group. Taken together, these results indicate that brain-infiltrating ILC2s play an indispensable role in brain tissue repair by mediating poststroke angiogenesis and vascular remodeling.

ILC2s promote initiation of angiogenesis by boosting angiogenic sprouting

Poststroke angiogenesis primarily initiates with angiogenic sprouting (Rust et al., 2019; Wälchli et al., 2023), including sprouting phase (conversion of endothelial cells into tip cells and leading the formation of side branches on the vascular surface)



and maturation phase (maturation of new lumens and junctions between endothelial cells) (Fang et al., 2023; Rust et al., 2019; Wälchli et al., 2023). To explore the connection between ILC2s and the initiation of angiogenesis, we look into the biological process of ILC2-induced endothelial changes using GO enrichment analysis (Fig. 4 A). A total of 17 GO items related to angiogenesis or vasculogenesis passed the threshold of significance (adjusted P < 0.005). Among which, seven items are related to sprouting angiogenesis. We further evaluate the transcriptomic level of tip cell-related gene between ILC2-transferred group and PBS group. For each group, endothelial cells that ranked high (top 0.1%, 0.5%, 1.0%, and 5.0%) in tip cell-related AUCell score are calculated for an average score (Fig. 4 B). The result showed higher tip cell-related AUCell score in endothelial cells compared with ILC2-transferred group.

To validate the role of ILC2s in angiogenic sprouting and tip cell formation, we chose day 5 after MCAO and ILC2 infusion as the observation time point based on: (1) previously reported experience indicating active angiogenesis 5 days after ischemic stroke (Williamson et al., 2021) and (2) ILC2s significantly accumulating in the brain at day 5 (Fig. 2). The identities of tip cells were confirmed by immunofluorescent staining of endothelial marker, CD31. Images of the cortical vascular structures at the ischemic hemisphere were generated by confocal z-stacks of 50-µm brain slices (Fig. 4, C and D). We observed considerable number of endothelial cells with filopodia in the brains of ILC2-treated group (Fig. 4, C and E). Meanwhile, the number of connected tip cell fronts were also higher in the ILC2-treated group (Fig. 4, D and F). In addition, we identified tip cells located near transferred EGFP-ILC2s (Fig. 4 G), indicating possible interactions between ILC2s and endothelial changes observed above.

ILC2s promote angiogenic sprouting in an α -CGRP-dependent manner

To look into the key mechanism between ILC2-mediated endothelial changes, we attempted to seek genes highly expressed by brain-infiltrating ILC2s, as well as exclusively upregulated by them. We intersected the DEGs from SMART-seq (brain 5d versus blood 5d, adjusted P < 0.05, log2FC > 2, 5962 genes in total) and significantly expressed genes identified from scRNAseq (adjusted P < 0.05, 1437 genes in total) of ILC2s, resulting in a mutual gene set of 150 intersecting genes (Fig. 5 A). Among these genes, six genes were identified as vascular remodeling-related genes encoding secretory proteins (Fig. 5 B), including (ranked by expression level): Calca encoding calcitonin and α-CGRP (Shi et al., 2022), Sema5a encoding semaphorin 5A, Sema3a encoding semaphorin 3A (Williams et al., 2007), Sema6d encoding semaphorin 6D (Epstein et al., 2015), and Npnt encoding nephronectin (Zhang et al., 2022). High expression of Calca and its encoding protein α-CGRP was validated by SMART-seq (Fig. 5 C) and immunofluorescence (Fig. 5 D).

Calca as the most significantly upregulated genes in activated ILC2s play a critical role in shaping type 2 inflammation in peripheral tissue (Nagashima et al., 2019; Wallrapp et al., 2019; Xu et al., 2019). Thus, we further investigated Calca and its role in ILC2-mediated angiogenesis after ischemic stroke. Calca gene

controls expression of calcitonin and α -CGRP by tissue-specific and cell-specific alternative RNA splicing. It is reported that activated ILC2s mainly produce α -CGRP rather than calcitonin (Xu et al., 2019). Rimegepant, an antagonist for CGRP receptor (Mulder et al., 2020), was used in the following *in vitro* experiments to test the role of ILC2s in α -CGRP-mediated angiogenesis. To elucidate the role of ILC2s and upregulated *Calca* during angiogenesis, we co-cultured ILC2s with mouse-derived microvascular endothelial cells (bEnd.3) in a noncontact manner (Fig. 5 E) to evaluate their ability to mediate angiogenesis.

Angiogenic sprouts are led by tip cells and elongated and supported by other endothelial cells (or stalk cells). Thus, both the ability of forming tip cells for sprouts and the ability of forming initial tubes are important for angiogenic sprouting. Thus, we evaluated the former by sprouting experiment using 3D endothelial spheroids and the latter by tubulogenesis experiment using 2D endothelial layers. ILC2s and α -CGRP equally enhanced sprouting ability of endothelial spheroids (Fig. 5, F–H); this effect was abolished with rimegepant applied. Tubulogenesis experiment also showed elevated tubulogenesis evoked by ILC2s and α -CGRP, which is blocked by rimegepant (Fig. 5, I–K). Thus, ILC2s and α -CGRP significantly promoted angiogenic sprouting, which can be abolished when α -CGRP is antagonized by rimegepant. These findings suggest that ILC2s promote angiogenic sprouting through α -CGRP.

As human ILC2s sometimes have different biological profile from mice ILC2s (Li et al., 2024), we isolated ILC2s from blood of a healthy human subject. Immunostaining showed expression of α-CGRP in human ILC2s (Fig. S4 B). The results of in vitro angiogenesis assays using HUVECs showed that human ILC2s can significantly promote sprouting (Fig. 5, L-N) and tubulogenesis (Fig. 5, O-Q) in human endothelial cells. To further validate the pro-angiogenic effects of human ILC2s mediated through α -CGRP, we compared the effects of human ILC2s on human endothelial cells under conditions involving either a CGRP receptor antagonist or α -CGRP antibody (Fig. S4 A). The results demonstrated that both inhibition of CGRP receptors on endothelial cell surfaces via rimegepant and neutralization of α-CGRP's downstream effects through fremanezumab (a humanized mAb for CGRP) effectively suppressed the proangiogenic activity of ILC2s (Fig. S4, C-H). Overall, these findings suggest that ILC2s promote angiogenic sprouting through α-CGRP in both mice and humans.

To further validate the role of α -CGRP in ILC2-mediated angiogenic sprouting, we utilized Calca-KO mice. By deleting exons 3 and 4 of the Calca gene, the complete mRNA-encoding α -CGRP could not be formed (Fig. 6 A). We isolated ILC2s from both WT and Calca-KO mice and used immunostaining to observe the distribution of α -CGRP (Fig. 6 B and Fig. S5). Consistent with our design, α -CGRP was not expressed in Calca-KO mice. In vitro angiogenesis assays using Calca-KO ILC2s (Fig. 6 C) did not show any sign of promoted sprouting (Fig. 6, D-F) and tubulogenesis (Fig. 6, G-I) in bEnd.3 cells when compared with control group (no ILC2s added). Furthermore, we i.v. transferred CFSE-labeled Calca-KO ILC2s and WT-ILC2s into WT mice 6 h after MCAO (Fig. 6 J). By day 5, immunofluorescent examination revealed that although Calca-KO ILC2s successfully reached the brain



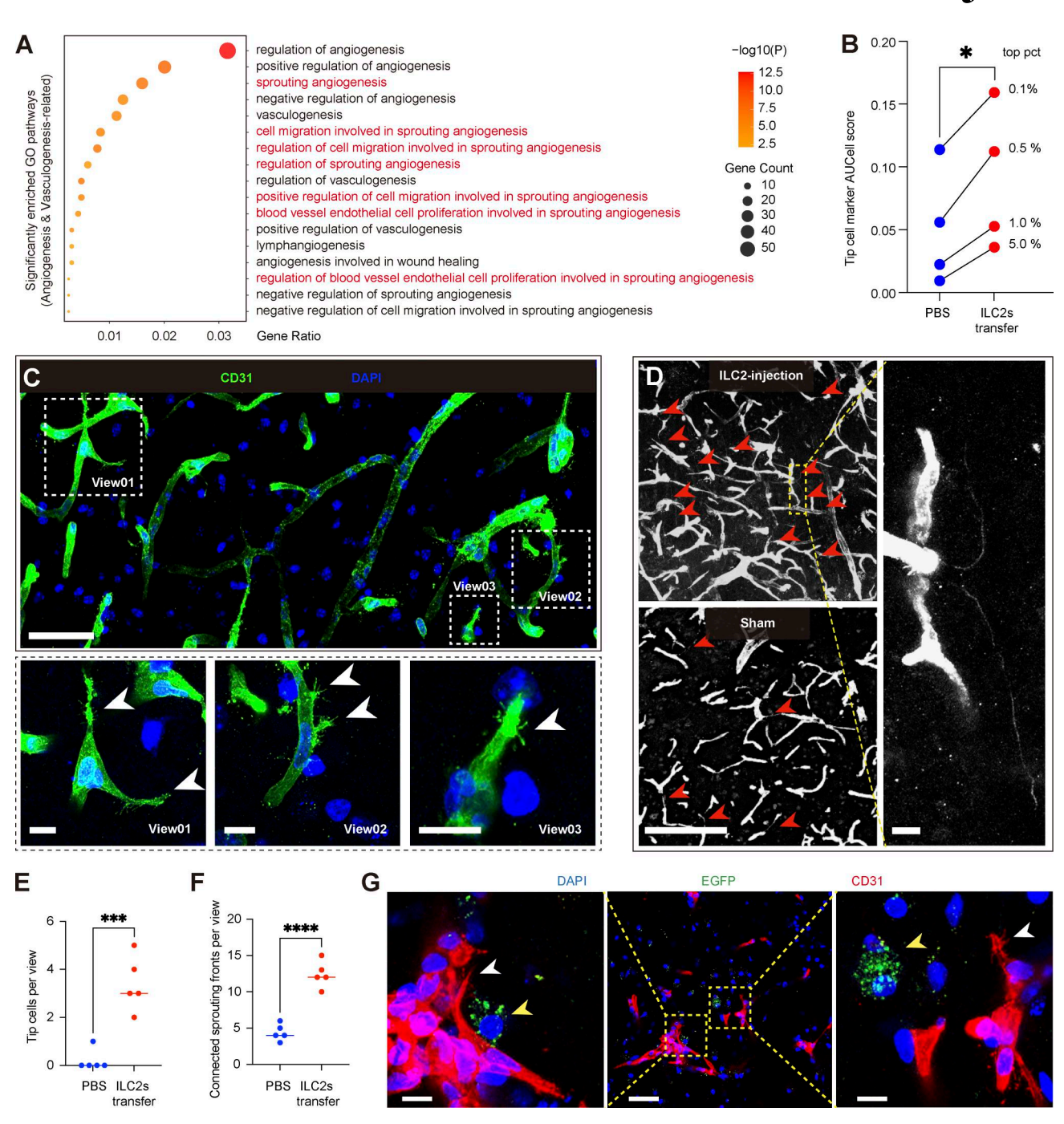


Figure 4. **ILC2s promote initiation of angiogenesis by boosting angiogenic sprouting. (A)** GOBP enrichment results based on the following pairwise comparisons: endothelial cells in ILC2-transferred group versus PBS group. **(B)** A comparison of AUCell scores for tip cells among top-scored (0.1%, 0.5%, 1%, and 5%) endothelial cells between ILC2s transfer group and PBS group, analyzed by two-sided, paired Student's t test. *P = 0.0103. **(C)** Immunofluorescence of peri-ischemic region at day 5 after MCAO and ILC2s transfer (images taken at 40×). White arrowheads: tip cells and endothelial cells with filopodia. Scale bars, 50 μ m (10 μ m for zoomed out). **(D)** Immunofluorescence of peri-ischemic region at day 5 after MCAO and ILC2s transfer (images taken at 20×). Red arrowheads: connected tip cell fronts. Scale bars, 100 μ m (10 μ m for zoomed out). **(E and F)** Morphometric quantification of angiogenic sprouting and by calculating the number of tip cells and endothelial cells with filopodia per 40× view (E), as well as number of connected tip cell fronts (F). Number of views = 5 per group. Each view from one mouse brain. The bar plots were analyzed by two-sided, unpaired Student's t test. All data represent biological replicates from two independent experiments. ***P = 0.0004; *****P < 0.0001. **(G)** Tip cells (white arrows) present near ILC2s (yellow arrows) peri-ischemic region at day 5 after MCAO and ILC2s transfer (images taken at 40×). Scale bars, 100 μ m (20 μ m for zoomed out).

(Fig. 6, K and L), they failed to promote the formation of tip cells (Fig. 6, M and N). These findings indicated that α -CGRP is indispensable for ILC2-mediated angiogenic sprouting after ischemic stroke in mice.

ILC2s derived α -CGRP promotes angiogenic sprouting and functional recovery though endothelial CGRP receptors α -CGRP is a neuropeptide with multiple beneficial roles in wound healing and inflammatory regulation, including as a



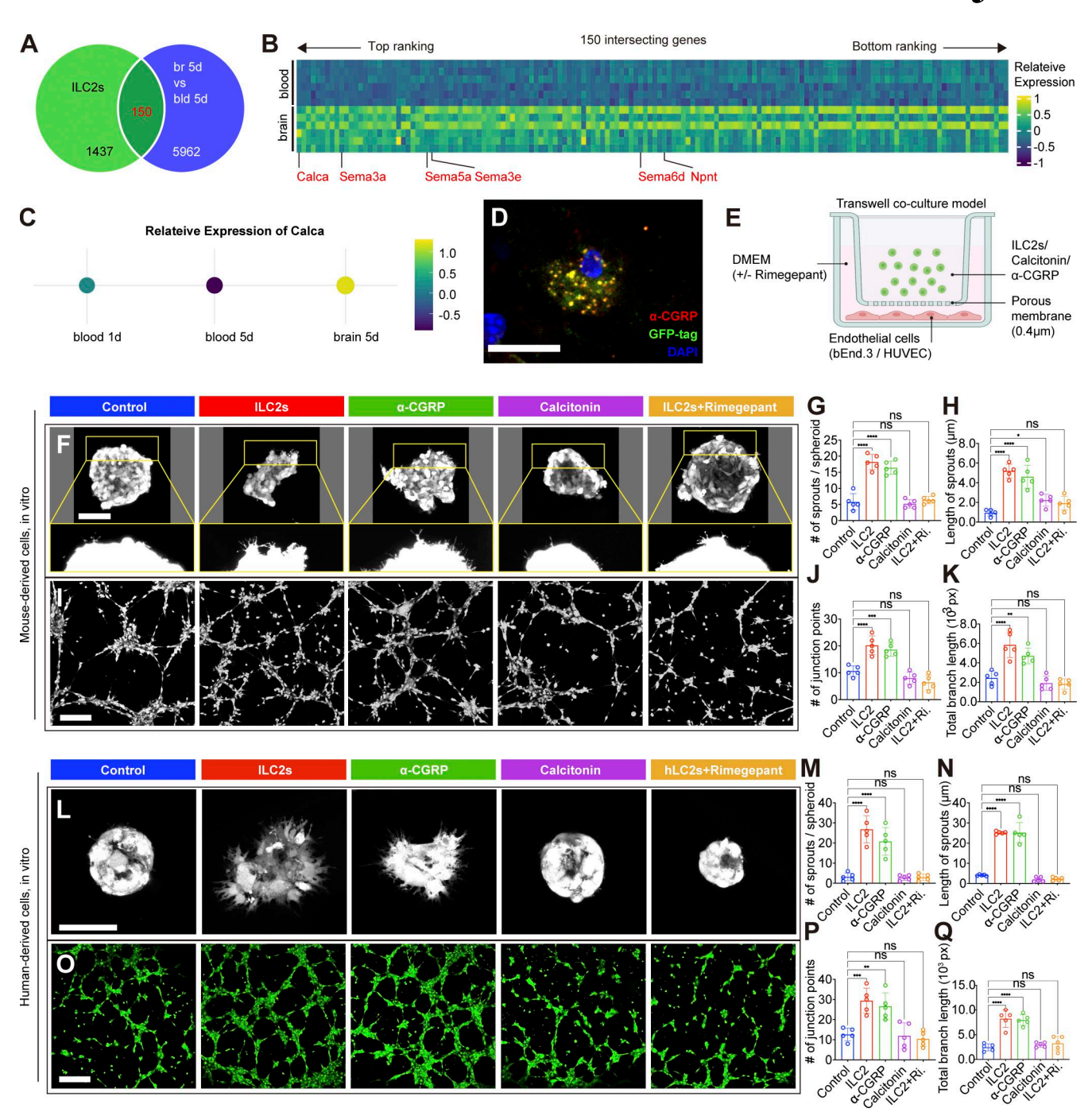


Figure 5. α-CGRP is crucial in ILC2-mediated angiogenic sprouting for both mice and human. (A) Venn plot of intersecting genes from top DEGs of ILC2s and DEGs between brain ILC2s versus blood ILC2s at day 5 after MCAO. (B) Heatmap displaying the relative expression of intersecting genes at day 5 after MCAO. Genes marked by red are potentially related to brain tissue remodeling. (C) Relative transcriptional expression of *Calca* at three states. (D) Immunofluorescence of a brain-infiltrating ILC2 5 days after MCAO and ILC2s transfer. Scale bar, 20 μm. (E) ILC2s were co-cultured with bEnd.3 cells without direct contact, separated by a 0.4-μm membrane (created with https://BioRender.com). (F-H) Mouse-derived cell assay: *In vitro* mouse endothelial spheroid sprouting experiment, quantification of the number and length of sprouts per spheroid in different treatment groups (n = 5). Ri, rimegepant. Data are shown as bar plots (SD, median), analyzed by one-way ANOVA with Tukey's multiple comparisons. *P = 0.0447; ****P < 0.0001; ns indicates P > 0.05. Scale bar, 100 μm. (I-K) Mouse-derived cell assay: *In vitro* mouse endothelial tube formation experiment, quantification of node number and in branch length of tubular structures different treatment groups (n = 5). Data are shown as bar plots (SD, median), analyzed by one-way ANOVA with Tukey's multiple comparisons. **P = 0.0004; ****P < 0.0001; ns indicates P > 0.05. Scale bar, 250 μm. (L-N) Human-derived cell assay: *In vitro* HUVEC sprouting experiment, quantification of node number and length of sprouts per spheroid (n = 5). Data are shown as bar plots (SD, median), analyzed by one-way ANOVA with Tukey's multiple comparisons. ****P < 0.0001; ns indicates P > 0.05. Scale bar, 100 μm. (O-Q) Human-derived cell assay: *In vitro* HUVEC tube formation experiment, quantification of node number and branch length of tubular structures (n = 5). Data are shown as bar plots (SD, median), analyzed by one-way ANOVA with Tukey's multiple comparisons. **P = 0.0020; *****P < 0.0001



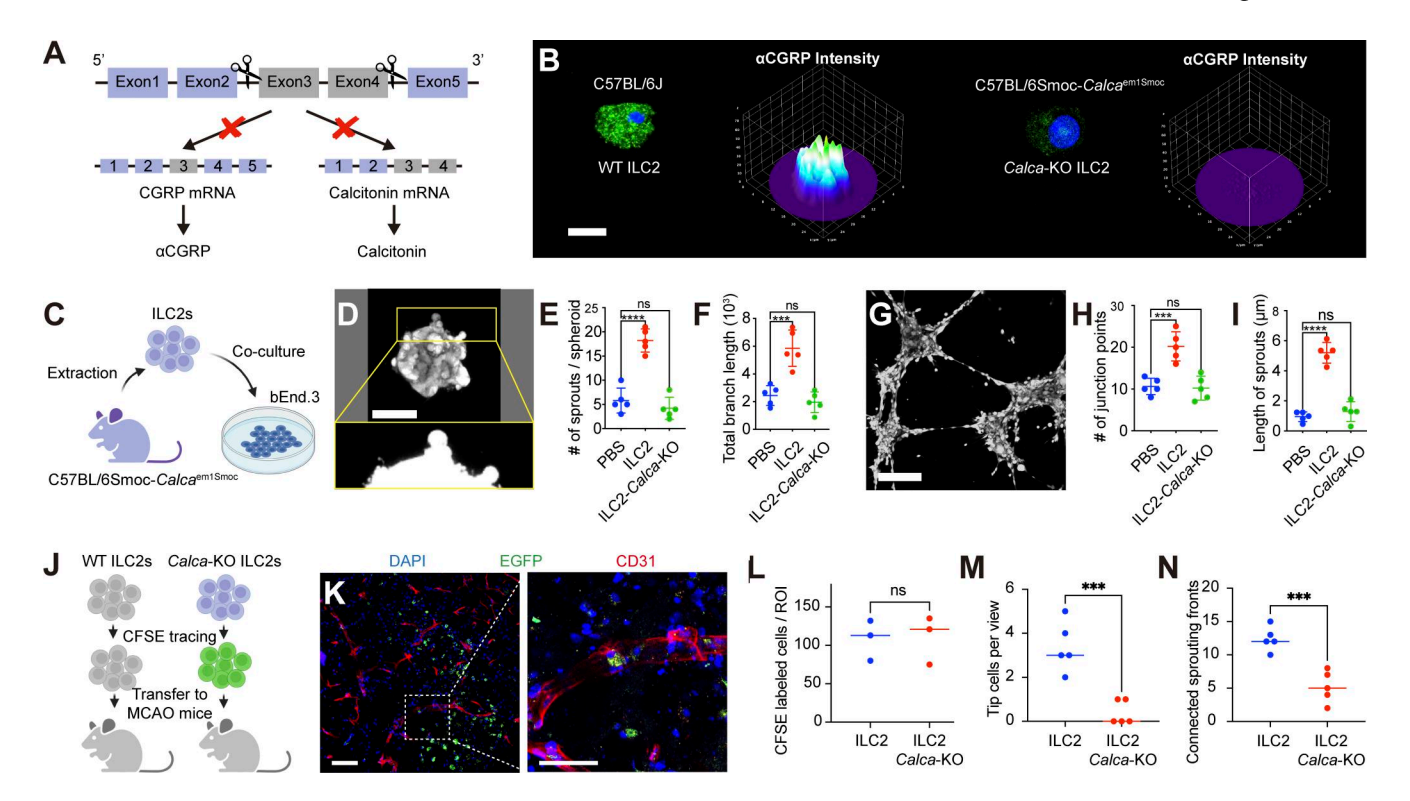


Figure 6. Loss of α-CGRP diminishes angiogenic sprouting after ischemic stroke. (A) Schematic illustration showing *in vivo* α-CGRP KO strategy (created with https://BioRender.com). (B) Immunofluorescence and 3D views of α-CGRP expression in ILC2s from WT mice and *Calca*-KO mice. Scale bar, 10 μm. (C) Schematic illustration showing *in vitro* co-culture experiment of ILC2s with bEnd.3 cells (created with https://BioRender.com). (D–F) Mouse-derived cell assay and quantified results of endothelial tube formation. Data are shown as bar plots (SD, median), analyzed by one-way ANOVA with Tukey's multiple comparisons. ***P = 0.0002; ****P < 0.0001; ns indicates P > 0.05. Scale bar, 100 μm. (G–I) Mouse-derived cell assay and quantified results of endothelial sprouting. Data are shown as bar plots (SD, median), analyzed by one-way ANOVA with Tukey's multiple comparisons. ***P = 0.0003; ****P < 0.0001; ns indicates P > 0.05. Scale bar, 250 μm. (J) Schematic illustration showing *in vivo* validation of angiogenic effect in WT or *Calca*-KO ILC2s at day 5 after MCAO and ILC2 infusion. *Calca*-KO ILC2s were labeled with CFSE (created with https://BioRender.com). (K and L) Immunofluorescence and quantification (*n* = 3) of labeled cell number in ischemic area of a mouse brain at day 5 after MCAO and CFSE-labeled *Calca*-KO ILC2s transfer, analyzed by two-sided, unpaired Student's *t* test. Data are from biological replicates and represent two independent experiments. P > 0.05. Scale bars, 100 μm (50 μm for zoomed out). (M and N) Morphometric quantification (*n* = 5) of angiogenic sprouting and by calculating the number of tip cells and endothelial cells with filopodia per 40× view, analyzed by two-sided, unpaired Student's *t* test. Data are from biological replicates and represent two independent experiments. ***P = 0.0007.

vasodilator, a regulator of IL-5 and amphiregulin, etc. To further validate the role of ILC2-derived α -CGRP in mediating angiogenic sprouting during poststroke functional recovery, it is necessary to specifically KO the CGRP receptor on cerebral vascular endothelial cells in mice, avoiding off-target effects on other cell types. The CGRP receptor belongs to the G proteincoupled receptor family and consists of three subunits: Calcitonin receptor-like receptor (CLR), a core transmembrane protein responsible for CGRP binding and signal transduction; receptor activity-modifying protein 1 (RAMP1), a single-pass transmembrane auxiliary protein that determines receptor ligand specificity and facilitates CLR membrane localization; and receptor component protein, an intracellular protein that enhances signal transduction efficiency. Among them, RAMP1 facilitates CLR trafficking from the endoplasmic reticulum to the cell membrane and ensures proper receptor expression (McLatchie et al., 1998). Additionally, its binding with CLR forms a high-affinity CGRP-binding site. Studies have shown that endothelial-specific RAMP1 KO in mice abolishes CGRP signaling, mimicking the effect of a CGRP receptor antagonist (Ding et al., 2022). Targeting RAMP1 usually offers

high specificity and efficiency in blocking CGRP receptor signaling.

We employed adeno-associated virus (AAV)-BR1, a serotype engineered by Körbelin et al. (2016) for selective transfection of mouse brain microvascular endothelial cells. A dual-AAV system: one vector (AAV-BR1-Streptococcus pyogenes Cas9 [SpCas9]) delivered guide RNA (gRNA) targeting the RAMP1 gene, while the other (AAV-BR1-sgRNA1_sgRNA2) encoded SpCas9 nuclease under the control of an endothelial-specific ICAM2 promoter. To minimize off-target effects, two gRNAs targeting distinct RAMP1 sequences were designed into the virus (Fig. 7 A).

For RAMP1 KO, mice were randomized into two groups receiving either control virus (AAV-BR1-SpCas9-EGFP) or dual viruses (AAV-BR1-sgRNA1_sgRNA2 + AAV-BR1-SpCas9). After 21 days of viral expression, MCAO was performed, and brains were analyzed at 5 days after stroke (Fig. 7 B). Before the formal experiments, a control AAV (AAV-BR1-SpCas9-EGFP) was used to verify cell type selectivity and protein expression at 21 days (Fig. 7 C). Immunofluorescence confirmed colocalization of EGFP with endothelial cells, representing effective transduction and ICAM2-driven SpCas9 expression. Significantly reduced RAMP1



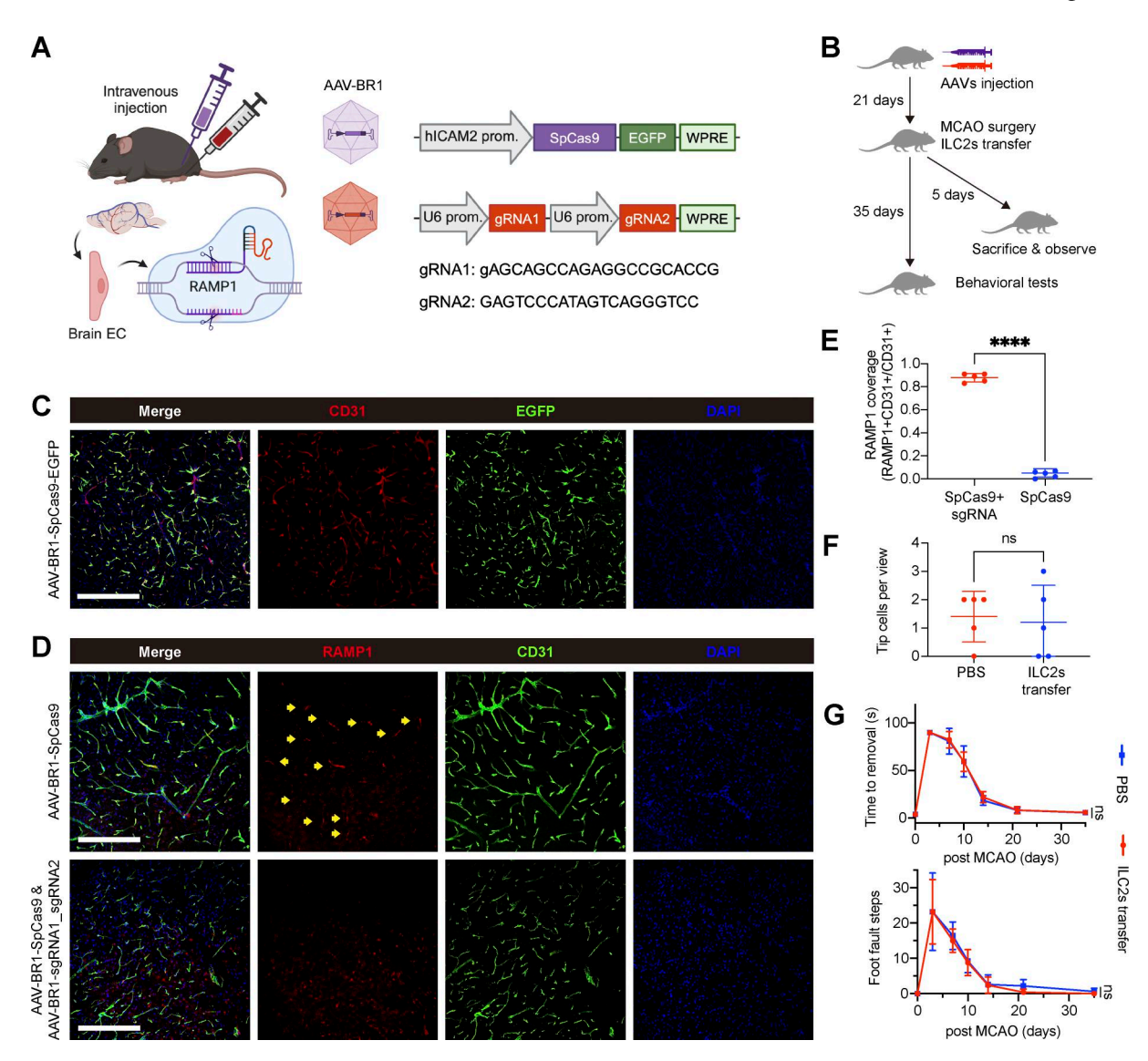


Figure 7. **ILC2-derived** α-CGRP promotes angiogenic sprouting and functional recovery though CGRP receptor on endothelial cells. (A) We employed dual AAV-BR1 vectors, with one vector carrying the hICAM2 promoter and SpCas9, and the other containing dual gRNAs targeting *Ramp1*. The mixed viruses were administered via femoral vein injection in mice, followed by a 21-day expression period prior to subsequent experiments (created with https://BioRender.com). (B) After 21 days of dual viral expression, MCAO was induced. Tissues were collected 5 days after MCAO for immunofluorescence staining. (C) EGFP expression after 21 days of dual viral expression. Scale bar, 100 μm. (D and E) Immunofluorescence and quantification of RAMP1 expression and its vascular coverage in cerebral blood vessels, analyzed by two-sided, unpaired Student's t test. Data are from biological replicates and represent two independent experiments. ****P < 0.0001. Scale bars, 100 μm. (F) Morphometric quantification of angiogenic sprouting and by calculating the number of tip cells and endothelial cells with filopodia per 40× view, analyzed by two-sided, unpaired Student's t test. Data are from biological replicates and represent two independent experiments. P > 0.05. (G) Behavioral tests of dual viral-transfected MCAO mice after PBS treatment and ILC2s transfer, analyzed by two-way ANOVA repeated measurement. Data are shown as line charts with error bars (SEM, median). P > 0.05.

coverage on endothelial cells in dual virus-transfected mice (Fig. 7, D and E). Meanwhile, RAMP1 expression in non-endothelial cells (e.g., neurons) was preserved (Fig. 7 D), consistent with reported CGRP receptor distribution in humans, primates, and rodents (Edvinsson et al., 2020; Eftekhari et al., 2013; Gimeno-Ferrer et al., 2022). No difference in tip cell density at day 5 after MCAO between ILC2-transferred and PBS-treated mice (Fig. 7 F) after RAMP1 KO, indicating abolished pro-angiogenic effects of ILC2s. No difference was observed in behavioral tests until 35 days after MCAO either (Fig. 7 G). These results demonstrated that dysfunction of endothelial CGRP

receptors disrupts α -CGRP/CGRP receptor–mediated angiogenic sprouting, thereby diminishing angiogenic sprouting promoted by ILC2-derived α -CGRP.

Discussion

In this study, we revealed ILC2s as a reparative candidate for cell-based therapy to promote tissue repair after ischemic stroke. The main findings can be summarized in two main points: (1) The infiltration of exogenous circulating ILC2s into the brain is mediated by CXCR1. (2) ILC2s facilitate sensorimotor



recovery through promoting angiogenic sprouting and tubulogenesis of capillary endothelial cells, which is mediated through α -CGRP.

Brain-infiltrating immune cells usually interact diversely with the immune environment and can have profound effect on tissue remodeling. Tregs, in addition to its immunosuppressive effects, we and others have previously demonstrated that braininfiltrating Tregs promote tissue repair following cerebral infarction in multiple aspects, particularly in white matter repair, including directly protecting oligodendrocytes (Zhang et al., 2018) or promoting their differentiation (Dombrowski et al., 2017), and indirectly repairing damaged white matter through microglia-mediated myelin regeneration (Shi et al., 2021). Similar to Tregs, the tissue-remodeling capabilities of braininfiltrating ILC2s also exhibit tissue specificity within the brain. Our scRNAseq of postMCAO brains revealed proportional changes and transcriptional changes in multiple cell types in addition to endothelial cells at day 14 after ILC2 injections (Fig. S4). The ability of ILC2 cells to promote type 2 immunity is likely to indirectly enhance tissue repair by modulating microglia and monocyte-derived macrophages to transition into the M2 phenotype, which is associated with pro-repair functions. Therefore, the protective and reparative roles of ILC2 in cerebral infarction and other neuroinflammatory conditions may manifest at different stages of inflammation, either directly or indirectly. However, unlike Tregs, ILC2s mature without the need for recombination activating gene-mediated TCR rearrangement (Ferreira et al., 2021; Gentek et al., 2013). The activation of ILC2s requires tissue-derived cytokines, such as IL-33 or IL-25, but is independent of antigen-specific receptors like T cells, enabling ILC2s to function in a rapid and board way (Tsou et al., 2022). Recent advances have been made in therapeutically administering ILC2s to treat patients with hematological malignancies without causing side effects like graft-versus-host disease, validating its promising role in cell-based therapy (Li et al., 2024).

Angiogenesis after ischemic stroke is a multistage process. During each stage, the endothelial cells are mediated by different molecular signals. Our study has uncovered a role of ILC2derived α -CGRP on initiation of angiogenic process. α -CGRP is a neuropeptide that is mainly secreted by peripheral nerves. The number of α -CGRP-positive neurons in the brain is limited, mainly locating within the amygdala. Thus, the concentration of α -CGRP in the brain is low. Abnormally concentrated α -CGRP is considered the major cause of migraine (Russo and Hay, 2023). Rimegepant, the small-molecule inhibitor of the CGRP receptor we used is a typical clinical treatment for migraine. It has been shown that CGRP receptor inhibitors are related to decreased blood flow during ischemic stroke and increased infarct volumes, possibly due to inhibition of CGRP-induced vascular relaxations (Mulder et al., 2020). Another important role of α-CGRP is as an inhibitor of ILC2s responses to alarmins and other positive regulators (Yang et al., 2024). The inhibitory effects include reduced cell proliferation (Xu et al., 2019; Yang et al., 2024) and less type 2 cytokine production (Nagashima et al., 2019; Yang et al., 2024). During type 2 innate immune responses, CGRP is a negative regulator that shapes ILC2s' responses to alarmins and neuropeptides through stimulating the

intracellular production of cAMP (Nagashima et al., 2019). Thus, when facing external stimulation, CGRP act as a feedback regulator against rapid waves of ILC2-related responses. In the context of brain injury, it is also crucial to have local type 2 inflammation in control, since continuous type 2 inflammation could cause pathological conditions, including excessive microglial activation and host death (Peng et al., 2022), or whole-body reactions, including the development of conditions that include asthma, allergic rhinitis, and other kinds of allergies (Mamuladze and Kipnis, 2023). Thus, CGRPdependent self-control mechanism could be useful in clinical translation of ILC2-based therapies, stabilizing the number of brain ILC2s to prevent the brain from overcolonized by ILC2s. Other questions regarding the multipotent effect of ILC2s on other stages of angiogenesis remain to be answered, calling for more detailed investigation into therapeutic angiogenesis after stroke.

As part of the innate immune system, ILC2 holds significant potential for clinical translation. First, our results indicate that ILC2s, upon entering the peripheral circulation of stroke patients, can infiltrate the brain in large numbers during the early poststroke period, demonstrating advantages in both responding speed and targeting specificity. Second, ILC2s exhibit multiple effects, including promoting tissue repair and modulating inflammation (Zheng et al., 2023), making them effective during both the acute and recovery phases of stroke. Additionally, despite the low abundance of ILC2 cells in human peripheral blood (Bartemes et al., 2014), current methods can effectively expand their numbers by several thousand-fold within weeks (Li et al., 2024). Merely 10 ml of peripheral blood can yield ILC2 cells at a level of 107, and pre-cryopreservation of these cells prior to the onset of stroke or other diseases can facilitate efficient utilization. In previous studies, both IL2-JES6-1 (Engelbertsen et al., 2015; Newland et al., 2017; Yu et al., 2021) and IL-33 (Cao et al., 2018; Stier et al., 2018) have been used to expand ILC2s. IL-33 as a broad-acting alarmin cytokine activates ILC2s, basophils, eosinophils, mast cells DCs, and CD4⁺ T cells (Drake and Kita, 2017). While anti-IL-33 antibody itepekimab has been tested in treating human airway inflammation, IL-33 has not been therapeutically applied to human subjects. Thus, considering its possible effects on other cells and its compatibility for clinical application, we used IL-33 merely for in vivo expansion to acquire abundant number of ILC2s for in vitro expansion. In contrast, low-dose IL-2 has been a widely tested and used treatment for human autoimmune diseases. IL2-JES6-1 mAb complex is a mAb complex that selectively targets IL2RA (Boyman et al., 2006; Yu et al., 2021). IL2-JES6-1 had been shown to selectively expand Tregs, which suppressed disease-related immune inflammation in a number of murine inflammatory and/or autoimmune models (Shevach, 2012). For future research, a more selective molecule should be developed for endogenous expansion of ILC2s, facilitating convenient and rapid clinical application.

In summary, our investigation elucidates the mechanisms and effects by which ILC2s infiltrate the brain to promote stroke recovery, thus highlighting the therapeutic potential of ILC2s in addressing current gaps in stroke treatment and warranting further clinical translation.



Our study has some limitations. The potential impact of ILC2derived α -CGRP on the central nervous system has not been thoroughly investigated. Our study observed that braininfiltrating ILC2s primarily aggregate at and around the infract zone, but it is possible that α -CGRP could diffuse to other brain regions through interstitial space or blood flow. While our findings suggest that the infiltration of ILC2s following i.v. administration is transient and that they do not persist in large numbers within the brain without sustained exogenous cytokine support, we cannot rule out the possibility that α -CGRP may cause short-term migraine-like side effects (Russo and Hay, 2023). Therefore, before advancing to further clinical studies, the potential neurological effects of ILC2-derived α -CGRP need to be explored in greater depth. Additionally, our study did not further assess other potential adverse effects of ILC2 infusion therapy on the central nervous system. Despite our single-cell sequencing analysis indicating no significant reduction in the number of neurons, BBB components, oligodendrocytes or their precursor cells, and no upregulation of apoptosis- or inflammation-related terms in cellular transcriptome, more comprehensive studies are needed. Previous research has shown that ILC2s mainly exert anti-inflammatory effects on neuroinflammation in the brain, but as a cell type that is naturally scarce in the brain, the effects of ILC2s after they enter the brain require further investigation. These limitations highlight the need for extensive preliminary research on the cell life cycle, intercellular interactions, and the cascade effects of effector molecules when selecting a new cell type for immunotherapy. Such research may even need to be conducted across different animal species.

Materials and methods

Animals

Young (8–10-wk-old) transgenic and WT male mice on a C57BL/6 background were used, which were all purchased from Shanghai Model Organisms Center, Inc. Transgenic strains were C57BL/6Smoc-Calca^{em1Smoc} (#NM-KO-190928) and B6.Cg-Tg(CAG-GFP)Smoc (#NM-TG-00005). All animals utilized for in vivo experiments were quartered in suitable temperature and humidity-controlled plastic cages with a 12 h light/dark period, where plentiful water and food were provided. Every endeavor was made to minimize animal suffering and the quantity of mice used. All animal procedures were authorized by the Institutional Ethics Committee of the Second Affiliated Hospital, School of Medicine, Zhejiang University, which also consented to National Institutes of Health Guide for the Care and Use of Laboratory Animals.

Murine models of transient MCAO

Transient MCAO model was induced as previously described (Zhang et al., 2019). Mice were deeply anesthetized with 1% pentobarbital and then secured onto a plastic board while they were unresponsive to tail pinch tests. After carefully separating the common carotid artery, external carotid artery (ECA), and internal carotid artery, a silicone-coated filament with its head was inserted into ECA via a small incision. Subsequently, the

filament was adjusted direction and advanced into internal carotid artery until resistance was perceived; thus, the original of the middle cerebral artery was blocked and transient cerebral ischemia was induced. The filament was left at that position for 60 min and withdrawn to restore cerebral blood flow; then, after which, the residual segment of ECA was knotted and the skin of the neck was sutured cautiously. 30% $O_2/70\%$ N2O was provided through nasal cannula to guarantee normal respiration, and the body temperature was maintained at 37.0 \pm 0.5°C during entire operation processes. Sham group mice underwent same operation without occlusion of middle cerebral artery. The mice were placed on a warming blanket after surgery until they regained consciousness from anesthesia. The surgical personals were unaware of the grouping of mice.

Intraperitoneal injection of IL-2/IL-2-Ab complex and IL-33

Recombinant murine IL-2 protein (abs04100; absin) and JES6-1 anti-mouse IL-2 mAbs (16-7022-85; eBioscience) were used to form IL2–JES6-1 complex. IL-2 protein was mixed with anti-IL-2 at a 2:1 M ratio (1 μ g of recombinant murine IL-2 protein and 5 μ g of anti-IL-2 mAbs) and incubated at 37°C for 30 min. IL2–JES6-1 complex or PBS control was intraperitoneally injected into mice at 6 h and 1, 2, 3, 7, 10, and 12 days after MCAO surgery. IL-33 (0.6 μ g/mouse/day, abs00985; Absin) was intraperitoneally injected into mice every 2 days for 7 days for in vivo expansion of ILC2s.

Single-cell suspension and flow cytometry analysis

Single-cell suspensions were prepared from bone marrow, blood, and brain. Isolated cells were resuspended at 1 × $10^6/ml$ and stained with fluorophore-labeled antibodies. For flow cytometry analysis and FACS of ILC2s from bone marrow, brain, and blood, the cells were stained with APC anti-mouse Lineage cocktail antibody (2 $\mu g/ml$, 51-9003632; BD Biosciences), BUV395 anti-mouse ST2 (2 $\mu g/ml$, 745738; BD Biosciences), PE-Cy7 anti-mouse CD127 (2 $\mu g/ml$, 560733; BD Biosciences), PE anti-mouse KLRG1 (2 $\mu g/ml$, 138407; BioLegend), PE-Cy7 anti-mouse GATA3 (2 $\mu g/ml$, 653819; BioLegend), and FITC anti-mouse CD45 (2 $\mu g/ml$, 103108; BioLegend).

Expansion, isolation, culturing, and in vivo infusion of mouse ILC2s

ILC2s were collected from the bone marrow and spleen of WT or transgenic mice. Briefly, an opening was made to an end of the femur. The femur was mechanically centrifuged at 10,000 rpm and subjected to density gradient centrifugation using Ficoll. We layered the blood on the top of Ficoll-Paque (GE Healthcare) and centrifuged it according to the manufacturer's instructions. The mononuclear cell fraction was aspirated and washed with PBS, and then the red blood cells were lysed. The ILC2s were initially selected using anti-Lin (CD11b, Gr1, CD3e, CD45R/B220, and Ter119) Abs (130-090-858; Miltenyi Biotec), followed by anti-biotin microbeads (Miltenyi Biotec). An AutoMACS separation column (Miltenyi Biotec) was used to remove Lin+ cells. Next, we used CD25 MicroBead Kit (130-091-072; Miltenyi Biotec) to collect CD25+ cells from Lin-cells. Isolated ILC2s and ILC2 progenitors were cultured in 10% FBS RPMI-1640 (Gibco) complete



medium containing 100 U/ml penicillin and 100 μ g/ml streptomycin (Biosharp) in the presence of IL-2 (10 ng/ml, abs04100; Absin), IL-7 (10 ng/ml, abs00975; Absin), IL-15 (10 ng/ml, abs01328; Absin), and IL-33 (10 ng/ml, abs00985; Absin). After 14 days, we sorted ILC2s using the FACS as described above. Next, we further cultured and expanded FACS-sorted ILC2s in the presence of IL-2, IL-7, and IL-15.

scRNA-seq and analysis

The single-cell suspensions were loaded into Chromium microfluidic chips with 3' chemistry and barcoded with a 10× Chromium Controller (10X Genomics). RNA from the barcoded cells was subsequently reverse transcribed and sequencing libraries constructed with reagents from a Chromium Single Cell 3' reagent kit (10X Genomics) according to the manufacturer's instructions. Sequencing was performed with Illumina (NovaSeq 6000) according to the manufacturer's instructions (Illumina). The fundamental processing and visualization of the scRNA-seq data were carried out using the Seurat package (version 4.4.0) within the R environment (version 4.0.2). To evaluate the expression level of a specified gene set, we employed AUCell (version 1.16.0).

SMART-seq of ILC2s

We i.v. transferred the isolated B6.Cg-Tg(CAG-GFP)Smoc ILC2s into WT mice 6 h after MCAO and collected them using FACS as described above at different time points. We collected the transferred ILC2s from the blood at day 1 (bld_1d, n=6) and day 5 (bld_5d, n=6), and also from the brain at day 5 after MCAO (br_5d, n=6) for RNA-seq. In addition, ILC2s directly from culture medium (base, n=5) were also included as a baseline control.

The SMART-seq procedure initiated with polyadenylated RNA templates from the samples. An oligo(dT) primer containing adapter sequences was used to prime first-strand cDNA synthesis, catalyzed by SMARTScribe Reverse Transcriptase. Upon reaching the 5' terminus of the RNA template, the intrinsic terminal transferase activity of SMART reverse transcriptase incorporated several additional nucleotides at the 3' end of the synthesized cDNA. A SMARTer oligonucleotide primerfeaturing adapter sequences at its 5' end and a complementary sequence to the extended 3' cDNA overhung at its 3' end—then annealed to the cDNA extension. The reverse transcriptase subsequently switched templates and continued elongation along this SMARTer oligonucleotide, thereby generating complete single-stranded cDNA molecules flanked by adapter sequences at both ends. These adapter-flanked cDNA products served as templates for PCR amplification using primers targeting the adapter sequences, ultimately yielding sufficient double-stranded cDNA for library construction and sequencing. The library was ready after end repair, A-tailing, adapter ligation, size selection, amplification, and purification.

After the library QC, it was pooled according to the effective concentration and the target data output required for the experiment, then subjected to Illumina sequencing, which produced 150-bp paired-end reads. The basic principle of the sequencing was "Sequencing by Synthesis," where fluorescently

labeled dNTPs, DNA polymerase, and adapter primers were added to the sequencing flow cell for amplification. As each sequencing cluster extended its complementary strand, the addition of each fluorescently labeled dNTP released a corresponding fluorescence signal. The sequencer captured these fluorescence signals and converted them into sequencing peaks through computer software, thereby obtaining the sequence information of the target fragment. Reads of all samples were aligned using HISAT2 (version 2.2.1). To minimize batch effects, ComBat_seq function from sva (version 3.42.0) was used to get a normalized count matrix. Genes differential expression analysis was performed by DESeq2 (1.34.0) between different groups.

Isolation and culturing of human ILC2s

Human ILC2s were isolated from a healthy donor's peripheral blood under ethical approval from the Second Affiliated Hospital of Zhejiang University Review Board (IR2019001143). We used a MACS-sorting kit for human (130-114-825; Miltenyi Biotec) to isolate ILC2s from human peripheral blood mononuclear cells according to the manufacturer's instructions. The medium for culturing human ILC2s was supplemented with human IL-2 (10 ng/ml, abs06177; Absin), IL-7 (10 ng/ml, abs05631; Absin), IL-15 (10 ng/ml, abs00818; Absin), and IL-33 (10 ng/ml, abs06263; Absin). Medium and cytokines were refreshed every 2 days by replacing half of the media containing cytokines. 4 wk later, the ILC2s were sorted using a FACSAriaTM (BD Bioscience). FACS-sorted ILC2s were used for following in vivo or in vitro experiments.

bEnd.3 and HUVEC: Spheroid sprouting assay and tube formation assay

Spheroid sprouting assay

bEnd.3 cells and HUVECs (1*106 cells/ml) were left overnight in 40 µl hanging drops of control medium to form spheroids as described previously. After 24 h, spheroids were harvested and embedded in 50-µl Phenol Red-free Standard Basement Membrane Matrix (M10262; LYNJUNE) in 24-well plates. The spheroid-containing gels were rapidly transferred into a humidified incubator (37°C, 5% CO₂). After 30 min, 0.5 ml control medium or conditioned medium were added per well. Co-culture of ILC2 and endothelial cells was performed with a transwell system, with the endothelial cells cultured at the bottom of the well and ILC2s at the top of the transwells. Mouse/human α-CGRP (HY-P0203A/HY-P1071; MCE), mouse/human calcitonin (HY-P77587/HY-P2273; MCE), rimegepant (Pfizer, Inc.), and fremanezumab (HY-P99019; MCE, for human-derived cells) were added to the bottom of the well after certain time (12 h for bEnd.3 cells, 8 h for HUVECs), the endothelial tubule formation was observed and photographed using a Leica DMi8 Inverted Microscope after staining with calcein AM (5 µM, C2012; Beyotime). The number of sprouts and cumulative length of sprouts per spheroid were quantified from five spheroids for each condition using Image J.

Tube formation assay

bEnd.3 cells or HUVECs were added to each well (2 \times 105 cells/ml) in 0.5 ml control medium or conditioned medium. After



certain time (12 h for bEnd.3 cells, 4 h for HUVECs), the endothelial tubule formation was observed and photographed using a Leica DMi8 Inverted Microscope after staining with Calcein AM. Total tube lengths were quantified using ImageJ. Branch points were manually counted.

Labeling new cells, evaluation of functioning blood vessels, and vascular permeability using lectin and Evans blue

To label proliferating cells after ischemic stroke, animals were intraperitoneally injected with BrdU (50 mg/kg) twice a day from day 4 to 10 after MCAO.

To visualize blood vessels, 30 μ l of 0.5 mg/ml EB (Sigma-Aldrich) and 100 μ l of tomato lectin DyLight 488 or 594 (L32470, L32471; Invitrogen) were injected i.v. before imaging. To capture dye extravasation, mice injected with a mixture of EB and lectin Dylight 488; EB was injected 30 min before sacrifice, and lectin was injected 5 min before sacrifice.

Immunofluorescence staining of brain slices and isolated cells

Brain slices were enucleated and fixed in 4% paraformaldehyde for 24 h at 4°C. The slices were then collected, blocked, and permeabilized in PBS containing 10% goat serum, 3% BSA, 1% Triton-X-100, and 0.2% Tween 20 for 1 h. Before immunostaining for BrdU, brain slices were incubated in 1 M HCL for 30 min at room temperature. Samples were then incubated with primary antibodies against goat CD31 (1:250, AF3628; R&D), goat α-CGRP (1:200, ab36001; Abcam), rabbit ZO-1 (1:200, ab221547; Abcam), and mouse BrdU (1:200, B35128; Invitrogen) overnight at 4°C, followed by incubation with fluorescenceconjugated cross-adsorbed secondary antibody (1:800, ALEXA FLUOR; Invitrogen) for 1 h, and then counterstained with DAPI with mounting media (ab104139; Abcam). For observation of in vitro-cultured cells, Evans blue leakage, and lectin 488/594, cells or brain sections were directly mounted on glass slides with 4',6-diamidino-2-phenylindole-containing mount G (Abcam) and covered with coverslips. Then the slices were examined by confocal microscopy (Leica DMi8). The recorded images were loaded into QuPath and were quantified by two independent observers blinded to grouping. Positively stained cells were electronically labeled with the software to avoid duplicated counting. The infarct area was identified as the region in which the majority of DAPI-stained nuclei were shrunken. The striatum areas were defined based on bright-field pre-image.

In vivo modulation of RAMP1 expression in cerebral endothelial cells using a dual-viral system

AAV vectors are among the primary tools for *in vivo* gene modulation due to their broad tissue tropism, non-pathogenicity, and low immunogenicity. In this study, we employed a dual-AAV system, packaging SpCas9 as a DNA endonuclease for double-strand cleavage and SpGuide for gRNA delivery. To achieve high specificity in transducing cerebral endothelial cells, we utilized the AAV-BR1 serotype, developed by Körbelin et al. (2016) (Augsburg University Hospital, Augsburg, Germany) through AAV2-based screening, which enables efficient and selective transduction of brain microvascular endothelia following i.v. administration (Körbelin et al., 2016).

Prior to transfection, AAV aliquots were thawed at 4°C and diluted 1:100 in pre-cooled PBS (original titer: 1 × 10¹³ gc/ml). Mice were anesthetized with 2.5% isoflurane, and the diluted viral solution (100 µl/mouse) was injected via the femoral vein. The experimental groups received either dual-AAV system, namely AAV-BR1[ssAAV.U6.ramp1_sgRNA1.U6.ramp1_sgRNA2.CAG.EGFP.WPRE.SV40 pA] (encoding two gRNAs targeting RAMP1); AAV-BR1[ssAAV.hICAM2.SpCas9] (expressing SpCas9 under the endothelial-specific hICAM2 promoter), or control system, namely AAV-BR1[ssAAV.hICAM2.EGFP.WPRE.SV40pA] (ex-

Behavioral tests

pressing EGFP only).

We employed the rotarod test and adhesive test, which have been previously reported to have high accuracy and sensitivity in estimating neurological deficits in rodents after stroke. Behavior test performers were blinded to the surgeon who established MCAO models, as well as the grouping of the mice. All behavior tests data were presented as the average ofthree duplicated trials per day, and a minimum interval between each trial was 15 min.

Foot fault test

Mice placed their paws on a wire while moving on an elevated grid surface. A foot fault was recorded when a paw slipped. Each animal was tested for three trials, lasting 1 min each. The data are expressed as the errors made by the contralateral limbs in every 50 steps.

Adhesive test

 2×3 -mm stickers were attached to the forelimb contralateral to ischemic hemisphere. The time taken to recognize and take away the stickers was recorded to assess the poststroke sensory function and motor ability of the mice individually. The maximum time for perception is 60 s and for stickers clearance is 120 s.

Online supplemental material

Fig. S1 shows the expression of classical markers for ILC2 identification in CD45 high cells. Fig. S2 shows the gating strategy and results of FACS and flow cytometry after MCAO and ILC2s transfer. Fig. S3 shows the SMART-seq results of transferred ILC2s. Fig. S4 shows that the pro-angiogenic effect of human-derived ILC2s can be inhibited by α -CGRP antibody or CGRP receptor antibody. Fig. S5 shows the colocalization and expression of α -CGRP with infused ILC2s.

Data availability

Data are available in the article itself and its supplementary materials. The SMART-seq data generated in this study have been deposited in the GEO database under accession code GSE302993. The scRNA-seq data generated in this study have been deposited in the GEO database under accession code GSE303092.

Acknowledgments

We would like to express our sincere gratitude to Zhihui Li from the Center for Basic and Translational Research of Second



Affiliated Hospital, School of Medicine, Zhejiang University, for her exceptional technical support with the FACS experiments. We also thank Zhuangchou Han and Siyuan Shen at LC Bio-Technology Co., Ltd. for their assistance with SMART-seq and bioinformatics analysis.

This work was supported by the National Natural Science Foundation of China (82322022, 82471296, 82271301 and 82471295). Natural Science Foundation of Zhejiang Province (LR23H250001).

Author contributions: An Ping: data curation, formal analysis, investigation, methodology, software, visualization, and writing—original draft, review, and editing. Fan Yang: formal analysis and investigation. Lingxiao Lu: formal analysis and investigation. Xiaotao Zhang: validation and visualization. Jianan Lu: formal analysis and visualization. Huaming Li: investigation, methodology, and validation. Yichen Gu: formal analysis and visualization. Jianmin Zhang: funding acquisition, supervision, and writing—review and editing. Ligen Shi: conceptualization, data curation, funding acquisition, investigation, project administration, supervision, and writing—review and editing.

Disclosures: The authors declare no competing interests exist.

Submitted: 3 October 2024 Revised: 2 June 2025 Accepted: 24 July 2025

References

- Agrawal, A., H. Balcı, K. Hanspers, S.L. Coort, M. Martens, D.N. Slenter, F. Ehrhart, D. Digles, A. Waagmeester, I. Wassink, et al. 2024. WikiPathways 2024: Next generation pathway database. *Nucleic Acids Res.* 52: D679–D689. https://doi.org/10.1093/nar/gkad960
- Aibar, S., C. González-Blas, T. Moerman, V. Huynh-Thu, H. Imrichova, G. Hulselmans, F. Rambow, J. Marine, P. Geurts, J. Aerts, et al. 2017. SCENIC: Single-cell regulatory network inference and clustering. Nat. Methods. 14:1083–1086. https://doi.org/10.1038/nmeth.4463
- Allen, J.E. 2023. IL-4 and IL-13: Regulators and effectors of wound repair. Annu. Rev. Immunol. 41:229-254. https://doi.org/10.1146/annurev-immunol-101921-041206
- Bando, J.K., H.-E. Liang, and R.M. Locksley. 2015. Identification and distribution of developing innate lymphoid cells in the fetal mouse intestine. Nat. Immunol. 16:153–160. https://doi.org/10.1038/ni.3057
- Bartemes, K.R., G.M. Kephart, S.J. Fox, and H. Kita. 2014. Enhanced innate type 2 immune response in peripheral blood from patients with asthma. *J. Allergy Clin. Immunol.* 134:671–678.e4. https://doi.org/10.1016/j.jaci
- Boyman, O., M. Kovar, M.P. Rubinstein, C.D. Surh, and J. Sprent. 2006. Selective stimulation of T cell subsets with antibody-cytokine immune complexes. *Science*. 311:1924–1927. https://doi.org/10.1126/science.1122927
- Campbell, L., C.R. Saville, P.J. Murray, S.M. Cruickshank, and M.J. Hardman. 2013. Local arginase 1 activity is required for cutaneous wound healing. J. Invest. Dermatol. 133:2461–2470. https://doi.org/10.1038/jid.2013.164
- Cao, Q., Y. Wang, Z. Niu, C. Wang, R. Wang, Z. Zhang, T. Chen, X.M. Wang, Q. Li, V.W.S. Lee, et al. 2018. Potentiating tissue-resident type 2 innate lymphoid cells by IL-33 to prevent renal ischemia-reperfusion injury. J. Am. Soc. Nephrol. 29:961–976. https://doi.org/10.1681/ASN.2017070774
- Cho, H.-S., A. Reboldi, J.A. Hall, and L.J. Berg. 2019. The Tec kinase ITK is essential for ILC2 survival and epithelial integrity in the intestine. *Nat. Commun.* 10:784. https://doi.org/10.1038/s41467-019-08699-9
- Deng, Z., T. Fan, C. Xiao, H. Tian, Y. Zheng, C. Li, and J. He. 2024. $TGF-\beta$ signaling in health, disease and therapeutics. *Signal Transduct. Target. Ther.* 9:61. https://doi.org/10.1038/s41392-024-01764-w

- Ding, W., L.L. Stohl, J. Saab, S. Azizi, X.K. Zhou, D. Mehta, and R.D. Granstein. 2022. Regulation of cutaneous immunity in vivo by calcitonin generelated peptide signaling through endothelial cells. *J. Immunol.* 208: 633–641. https://doi.org/10.4049/jimmunol.2100139
- Dombrowski, Y., T. O'Hagan, M. Dittmer, R. Penalva, S.R. Mayoral, P. Bankhead, S. Fleville, G. Eleftheriadis, C. Zhao, M. Naughton, et al. 2017. Regulatory T cells promote myelin regeneration in the central nervous system. *Nat. Neurosci.* 20:674–680. https://doi.org/10.1038/nn.4528
- Drake, L.Y., and H. Kita. 2017. IL-33: Biological properties, functions, and roles in airway disease. *Immunol. Rev.* 278:173-184. https://doi.org/10.1111/imr.12552
- Edvinsson, L., A.-S. Grell, and K. Warfvinge. 2020. Expression of the CGRP family of neuropeptides and their receptors in the trigeminal ganglion. J. Mol. Neurosci. 70:930–944. https://doi.org/10.1007/s12031-020-01493-z
- Eftekhari, S., C.A. Salvatore, R.C. Gaspar, R. Roberts, S. O'Malley, Z. Zeng, and L. Edvinsson. 2013. Localization of CGRP receptor components, CGRP, and receptor binding sites in human and rhesus cerebellar cortex. Cerebellum. 12:937-949. https://doi.org/10.1007/s12311-013-0509-4
- Engelbertsen, D., A.C. Foks, N. Alberts-Grill, F. Kuperwaser, T. Chen, J.A. Lederer, P. Jarolim, N. Grabie, and A.H. Lichtman. 2015. Expansion of CD25⁺ innate lymphoid cells reduces atherosclerosis. Arterioscler. Thromb. Vasc. Biol. 35:2526-2535. https://doi.org/10.1161/ATVBAHA.115.306048
- Epstein, J.A., H. Aghajanian, and M.K. Singh. 2015. Semaphorin signaling in cardiovascular development. *Cell Metab.* 21:163–173. https://doi.org/10 .1016/j.cmet.2014.12.015
- Fang, J., Z. Wang, and C.-Y. Miao. 2023. Angiogenesis after ischemic stroke. Acta Pharmacol. Sin. 44:1305–1321. https://doi.org/10.1038/s41401-023-01061-2
- Ferreira, A.C.F., A.C.H. Szeto, M.W.D. Heycock, P.A. Clark, J.A. Walker, A. Crisp, J.L. Barlow, S. Kitching, A. Lim, M. Gogoi, et al. 2021. RORα is a critical checkpoint for T cell and ILC2 commitment in the embryonic thymus. Nat. Immunol. 22:166-178. https://doi.org/10.1038/s41590-020-00833-w
- Fung, I.T.H., P. Sankar, Y. Zhang, L.S. Robison, X. Zhao, S.S. D'Souza, A.E. Salinero, Y. Wang, J. Qian, M.L. Kuentzel, et al. 2020. Activation of group 2 innate lymphoid cells alleviates aging-associated cognitive decline. J. Exp. Med. 217:e20190915. https://doi.org/10.1084/jem.20190915
- Gadani, S.P., I. Smirnov, A.T. Wiltbank, C.C. Overall, and J. Kipnis. 2017. Characterization of meningeal type 2 innate lymphocytes and their response to CNS injury. J. Exp. Med. 214:285–296. https://doi.org/10 .1084/jem.20161982
- Gentek, R., J.M. Munneke, C. Helbig, B. Blom, M.D. Hazenberg, H. Spits, and D. Amsen. 2013. Modulation of signal strength switches notch from an inducer of T cells to an inducer of ILC2. Front. Immunol. 4:334. https:// doi.org/10.3389/fimmu.2013.00334
- Ghaedi, M., C.A. Steer, I. Martinez-Gonzalez, T.Y.F. Halim, N. Abraham, and F. Takei. 2016. Common-lymphoid-progenitor-independent pathways of innate and T lymphocyte development. Cell Rep. 15:471–480. https:// doi.org/10.1016/j.celrep.2016.03.039
- Ghaedi, M., and F. Takei. 2021. Innate lymphoid cell development. J. Allergy Clin. Immunol. 147:1549–1560. https://doi.org/10.1016/j.jaci.2021.03.009
- Gimeno-Ferrer, F., A. Eitner, R. Bauer, A. Lehmenkühler, M.-L. Edenhofer, M. Kress, H.-G. Schaible, and F. Richter. 2022. From spreading depolarization to epilepsy with neuroinflammation: The role of CGRP in cortex. Exp. Neurol. 356:114152. https://doi.org/10.1016/j.expneurol.2022.114152
- Hayakawa, K., L.D.D. Pham, A.T. Som, B.J. Lee, S. Guo, E.H. Lo, and K. Arai. 2011. Vascular endothelial growth factor regulates the migration of oligodendrocyte precursor cells. J. Neurosci. 31:10666–10670. https://doi .org/10.1523/JNEUROSCI.1944-11.2011
- Hernández-Torres, D.C., and C. Stehle. 2022. Embryonic ILC-poiesis across tissues. Front. Immunol. 13:1040624. https://doi.org/10.3389/fimmu.2022.1040624
- Hinks, T.S.C., E. Marchi, M. Jabeen, M. Olshansky, A. Kurioka, T.J. Pediongco, B.S. Meehan, L. Kostenko, S.J. Turner, A.J. Corbett, et al. 2019. Activation and in vivo evolution of the MAIT cell transcriptome in mice and humans reveals tissue repair functionality. *Cell Rep.* 28:3249–3262.e5. https://doi.org/10.1016/j.celrep.2019.07.039
- Ikawa, T., K. Masuda, M. Lu, N. Minato, Y. Katsura, and H. Kawamoto. 2004. Identification of the earliest prethymic T-cell progenitors in murine fetal blood. Blood. 103:530–537. https://doi.org/10.1182/blood-2003-06-1797
- Jackson, D.J., H. Makrinioti, B.M.J. Rana, B.W.H. Shamji, M.B. Trujillo-Torralbo, J. Footitt, D.-R. Jerico, A.G. Telcian, A. Nikonova, J. Zhu, et al. 2014. IL-33-dependent type 2 inflammation during rhinovirus-induced asthma



- exacerbations in vivo. *Am. J. Respir. Crit. Care Med.* 190:1373–1382. https://doi.org/10.1164/rccm.201406-1039OC
- Körbelin, J., G. Dogbevia, S. Michelfelder, D.A. Ridder, A. Hunger, J. Wenzel, H. Seismann, M. Lampe, J. Bannach, M. Pasparakis, et al. 2016. A brain microvasculature endothelial cell-specific viral vector with the potential to treat neurovascular and neurological diseases. *EMBO Mol. Med.* 8: 609–625. https://doi.org/10.15252/emmm.201506078
- Lai, D., J. Tang, L. Chen, E.K. Fan, M.J. Scott, Y. Li, T.R. Billiar, M.A. Wilson, X. Fang, Q. Shu, and J. Fan. 2018. Group 2 innate lymphoid cells protect lung endothelial cells from pyroptosis in sepsis. *Cell Death Dis.* 9:369. https://doi.org/10.1038/s41419-018-0412-5
- Leitch, V.D, K.I. Strudwick, L.A. Matthaei, and A.J. Cowin. 2009. IL-5-over-expressing mice exhibit eosinophilia and altered wound healing through mechanisms involving prolonged inflammation. *Immunol. Cell Biol.* 87:131–140. https://doi.org/10.1038/icb.2008.72
- Li, Z., R. Ma, H. Tang, J. Guo, Z. Shah, J. Zhang, N. Liu, S. Cao, G. Marcucci, D. Artis, et al. 2024. Therapeutic application of human type 2 innate lymphoid cells via induction of granzyme B-mediated tumor cell death. Cell. 187:624–641.e23. https://doi.org/10.1016/j.cell.2023.12.015
- Liu, M., D. Wang, L. Xu, Y. Pan, H. Huang, M. Li, and Q. Liu. 2024. Group 2 innate lymphoid cells suppress neuroinflammation and brain injury following intracerebral hemorrhage. *J. Cereb. Blood Flow Metab.* 44: 355–366. https://doi.org/10.1177/0271678X231208168
- Mamuladze, T., and J. Kipnis. 2023. Type 2 immunity in the brain and brain borders. Cell. Mol. Immunol. 20:1290-1299. https://doi.org/10.1038/ s41423-023-01043-8
- McLatchie, L.M., N.J. Fraser, M.J. Main, A. Wise, J. Brown, N. Thompson, R. Solari, M.G. Lee, and S.M. Foord. 1998. RAMPs regulate the transport and ligand specificity of the calcitonin-receptor-like receptor. *Nature*. 393:333–339. https://doi.org/10.1038/30666
- Milacic, M., D. Beavers, P. Conley, C. Gong, M. Gillespie, J. Griss, R. Haw, B. Jassal, L. Matthews, B. May, et al. 2024. The reactome pathway knowledgebase 2024. Nucleic Acids Res. 52:D672–D678. https://doi.org/10.1093/nar/gkad1025
- Monticelli, L.A., G.F. Sonnenberg, M.C. Abt, T. Alenghat, C.G.K. Ziegler, T.A. Doering, J.M. Angelosanto, B.J. Laidlaw, C.Y. Yang, T. Sathaliyawala, et al. 2011. Innate lymphoid cells promote lung-tissue homeostasis after infection with influenza virus. *Nat. Immunol.* 12:1045–1054. https://doi.org/10.1031/ni.2131
- Mulder, I.A., M. Li, T. de Vries, T. Qin, T. Yanagisawa, K. Sugimoto, A. van den Bogaerdt, A.H.J. Danser, M.J.H. Wermer, A.M.J.M. van den Maagdenberg, et al. 2020. Anti-migraine calcitonin gene-related peptide receptor antagonists worsen cerebral ischemic outcome in mice. Ann. Neurol. 88:771-784. https://doi.org/10.1002/ana.25831
- Nagashima, H., T. Mahlakoiv, H.-Y. Shih, F.P. Davis, F. Meylan, Y. Huang, O.J. Harrison, C. Yao, Y. Mikami, J.F. Urban Jr., et al. 2019. Neuropeptide CGRP limits group 2 innate lymphoid cell responses and constrains type 2 inflammation. *Immunity*. 51:682–695.e6. https://doi.org/10.1016/j.immuni.2019.06.009
- Newland, S.A., S. Mohanta, M. Clément, S. Taleb, J.A. Walker, M. Nus, A.P. Sage, C. Yin, D. Hu, L.L. Kitt, et al. 2017. Type-2 innate lymphoid cells control the development of atherosclerosis in mice. *Nat. Commun.* 8: 15781. https://doi.org/10.1038/ncomms15781
- Peng, J., C.B. Sy, J.J. Ponessa, A.D. Lemenze, C.M. Hernandez, J.M. Inclan-Rico, A. Sawhney, H.G. Federman, K. Chavan, V. Espinosa, et al. 2022. Monocytes maintain central nervous system homeostasis following helminth-induced inflammation, Proc. Natl. Acad. Sci. USA. 119: e2201645119. https://doi.org/10.1073/pnas.2201645119
- Puttur, F., L. Denney, L.G. Gregory, J. Vuononvirta, R. Oliver, L.J. Entwistle, S.A. Walker, M.B. Headley, E.J. McGhee, J.E. Pease, et al. 2019. Pulmonary environmental cues drive group 2 innate lymphoid cell dynamics in mice and humans. Sci. Immunol. 4:eaav7638. https://doi.org/10.1126/ sciimmunol.aav7638
- Ricardo-Gonzalez, R.R., S.J. Van Dyken, C. Schneider, J. Lee, J.C. Nussbaum, H.-E. Liang, D. Vaka, W.L. Eckalbar, A.B. Molofsky, D.J. Erle, and R.M. Locksley. 2018. Tissue signals imprint ILC2 identity with anticipatory function. *Nat. Immunol.* 19:1093–1099. https://doi.org/10.1038/s41590-018-0201-4
- Russo, A.F., and D.L. Hay. 2023. CGRP physiology, pharmacology, and therapeutic targets: Migraine and beyond. *Physiol. Rev.* 103:1565–1644. https://doi.org/10.1152/physrev.00059.2021
- Rust, R., L. Grönnert, R.Z. Weber, G. Mulders, and M.E. Schwab. 2019. Refueling the ischemic CNS: Guidance molecules for vascular repair. Trends Neurosci. 42:644-656. https://doi.org/10.1016/j.tins.2019.05.006
- Schneider, C., J. Lee, S. Koga, R.R. Ricardo-Gonzalez, J.C. Nussbaum, L.K. Smith, S.A. Villeda, H.-E. Liang, and R.M. Locksley. 2019. Tissue-

- resident group 2 innate lymphoid cells differentiate by layered ontogeny and in situ perinatal priming. *Immunity*. 50:1425–1438.e5. https://doi.org/10.1016/j.immuni.2019.04.019
- Shevach, E.M. 2012. Application of IL-2 therapy to target T regulatory cell function. Trends Immunol. 33:626-632. https://doi.org/10.1016/j.it.2012 .07.007
- Shi, K., D.-C. Tian, Z.-G. Li, A.F. Ducruet, M.T. Lawton, and F.-D. Shi. 2019. Global brain inflammation in stroke. *Lancet. Neurol.* 18:1058–1066. https://doi.org/10.1016/S1474-4422(19)30078-X
- Shi, L., Z. Sun, W. Su, F. Xu, D. Xie, Q. Zhang, X. Dai, K. Iyer, T.K. Hitchens, L.M. Foley, et al. 2021. Treg cell-derived osteopontin promotes microglia-mediated white matter repair after ischemic stroke. *Immunity*. 54:1527-1542.e8. https://doi.org/10.1016/j.immuni.2021.04.022
- Shi, Y., L. Zhang, H. Pu, L. Mao, X. Hu, X. Jiang, N. Xu, R.A. Stetler, F. Zhang, X. Liu, et al. 2016. Rapid endothelial cytoskeletal reorganization enables early blood-brain barrier disruption and long-term ischaemic reperfusion brain injury. Nat. Commun. 7:10523. https://doi.org/10.1038/ncomms10523
- Shi, Z., S. Wang, J. Deng, and Z. Gong. 2022. Neural peptide α-CGRP coregulated angiogenesis and osteogenesis via promoting the cross-talk between mesenchymal stem cells and endothelial cells. Biomed. Res. Int. 2022;1585840. https://doi.org/10.1155/2022/1585840
- Stier, M.T., J. Zhang, K. Goleniewska, J.Y. Cephus, M. Rusznak, L. Wu, L. Van Kaer, B. Zhou, D.C. Newcomb, and R.S. Peebles Jr. 2018. IL-33 promotes the egress of group 2 innate lymphoid cells from the bone marrow. J. Exp. Med. 215:263-281. https://doi.org/10.1084/jem.20170449
- Tsou, A.M., H. Yano, C.N. Parkhurst, T. Mahlakõiv, C. Chu, W. Zhang, Z. He, K.J. Jarick, C. Zhong, G.G. Putzel, et al. 2022. Neuropeptide regulation of non-redundant ILC2 responses at barrier surfaces. *Nature* 611:787–793. https://doi.org/10.1038/s41586-022-05297-6
- Vivier, E., D. Artis, M. Colonna, A. Diefenbach, J.P. Di Santo, G. Eberl, S. Koyasu, R.M. Locksley, A.N.J. McKenzie, R.E. Mebius, et al. 2018. Innate lymphoid cells: 10 Years on. Cell. 174:1054–1066. https://doi.org/10.1016/j.cell.2018.07.017
- Wälchli, T., J. Bisschop, P. Carmeliet, G. Zadeh, P.P. Monnier, K. De Bock, and I. Radovanovic. 2023. Shaping the brain vasculature in development and disease in the single-cell era. *Nat. Rev. Neurosci.* 24:271–298. https://doi.org/10.1038/s41583-023-00684-y
- Wallrapp, A., P.R. Burkett, S.J. Riesenfeld, S.-J. Kim, E. Christian, R.-E.E. Abdulnour, P.I. Thakore, A. Schnell, C. Lambden, R.H. Herbst, et al. 2019. Calcitonin gene-related peptide negatively regulates alarmin-driven type 2 innate lymphoid cell responses. *Immunity*. 51:709–723.e6. https://doi.org/10.1016/j.immuni.2019.09.005
- Wang, S., and S.A. van de Pavert. 2022. Innate lymphoid cells in the central nervous system. Front. Immunol. 13:837250. https://doi.org/10.3389/ fimmu.2022.837250
- Williams, A., G. Piaton, M.-S. Aigrot, A. Belhadi, M. Théaudin, F. Petermann, J.L. Thomas, B. Zalc, and C. Lubetzki. 2007. Semaphorin 3A and 3F: Key players in myelin repair in multiple sclerosis? *Brain*. 130:2554–2565. https://doi.org/10.1093/brain/awm202
- Williamson, M.R., C.J.A. Fuertes, A.K. Dunn, M.R. Drew, and T.A. Jones. 2021. Reactive astrocytes facilitate vascular repair and remodeling after stroke. Cell Rep. 35:109048. https://doi.org/10.1016/j.celrep.2021.109048
- Xing, Y., H. Stefanski, D.W. Bruce, K.L. Hippen, J.M. Coghill, K. McKinnon, S. Reisdorf, B. Blazar, and J.S. Serody. 2017. A novel process for the expansion of functional human ILC2 cells for GCHD prevention. *Blood*. 130: 4432. https://doi.org/10.1182/blood.V130.Suppl_1.4432.4432
- Xu, H., J. Ding, C.B.M. Porter, A. Wallrapp, M. Tabaka, S. Ma, S. Fu, X. Guo, S.J. Riesenfeld, C. Su, et al. 2019. Transcriptional atlas of intestinal immune cells reveals that neuropeptide alpha-CGRP modulates group 2 innate lymphoid cell responses. *Immunity*. 51:696–708.e9. https://doi.org/10.1016/j.immuni.2019.09.004
- Yang, Z., Y. Liu, Y. Xiang, R. Chen, L. Chen, S. Wang, L. Lv, M. Zang, N. Zhou, S. Li, et al. 2024. ILC2-derived CGRP triggers acute inflammation and nociceptive responses in bacterial cystitis. Cell Rep. 43:114859. https://doi.org/10.1016/j.celrep.2024.114859
- Yu, X., S.A. Newland, T.X. Zhao, Y. Lu, A.S. Sage, Y. Sun, R.S. Sriranjan, M.K.L. Ma, B.Y.H. Lam, M. Nus, et al. 2021. Innate lymphoid cells promote recovery of ventricular function after myocardial infarction. J. Am. Coll. Cardiol. 78:1127-1142. https://doi.org/10.1016/j.jacc.2021.07 018
- Zaiss, D.M.W., W.C. Gause, L.C. Osborne, and D. Artis. 2015. Emerging functions of amphiregulin in orchestrating immunity, inflammation, and tissue repair. *Immunity*. 42:216–226. https://doi.org/10 .1016/j.immuni.2015.01.020



- Zhang, H., Y. Xia, Q. Ye, F. Yu, W. Zhu, P. Li, Z. Wei, Y. Yang, Y. Shi, A.W. Thomson, et al. 2018. In vivo expansion of regulatory T cells with IL-2/IL-2 antibody complex protects against transient ischemic stroke. *J. Neurosci.* 38:10168–10179. https://doi.org/10.1523/JNEUROSCI.3411-17.2018
- Zhang, Q., W. Zhu, F. Xu, X. Dai, L. Shi, W. Cai, H. Mu, T.K. Hitchens, L.M. Foley, X. Liu, et al. 2019. The interleukin-4/PPARγ signaling axis promotes oligodendrocyte differentiation and remyelination after brain injury. PLoS Biol. 17:e3000330. https://doi.org/10.1371/journal.pbio.3000330
- Zhang, Y., D. Wang, Z. Zhao, L. Liu, G. Xia, T. Ye, Y. Chen, C. Xu, X. Jin, and C. Shen. 2022. Nephronectin promotes cardiac repair post myocardial infarction via activating EGFR/JAK2/STAT3 pathway. *Int. J. Med. Sci.* 19: 878–892. https://doi.org/10.7150/ijms.71780
- Zheng, P., Y. Xiu, Z. Chen, M. Yuan, Y. Li, N. Wang, B. Zhang, X. Zhao, M. Li, Q. Liu, et al. 2023. Group 2 innate lymphoid cells resolve neuro-inflammation following cerebral ischaemia. Stroke Vasc. Neurol. 8: 424–434. https://doi.org/10.1136/svn-2022-001919



Supplemental material

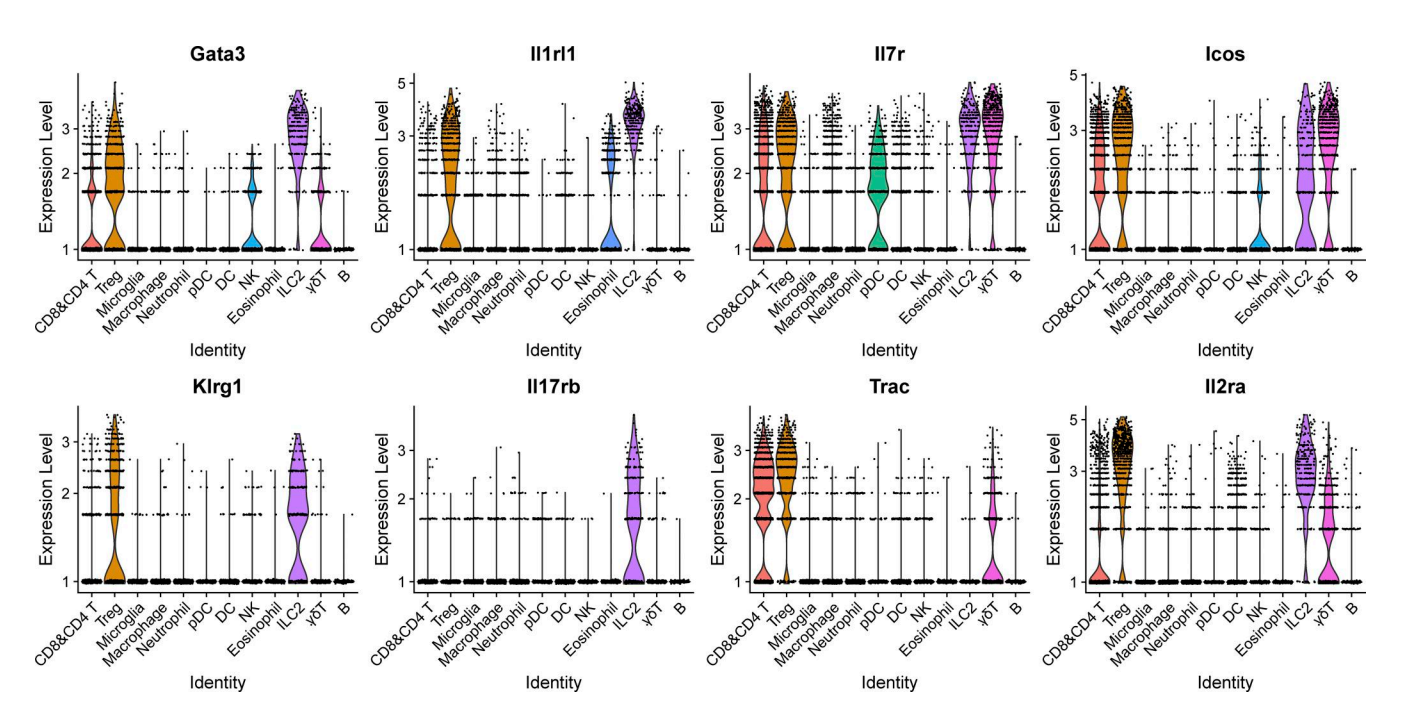


Figure S1. Expression of classical markers for ILC2 identification in CD45^{high} cells.



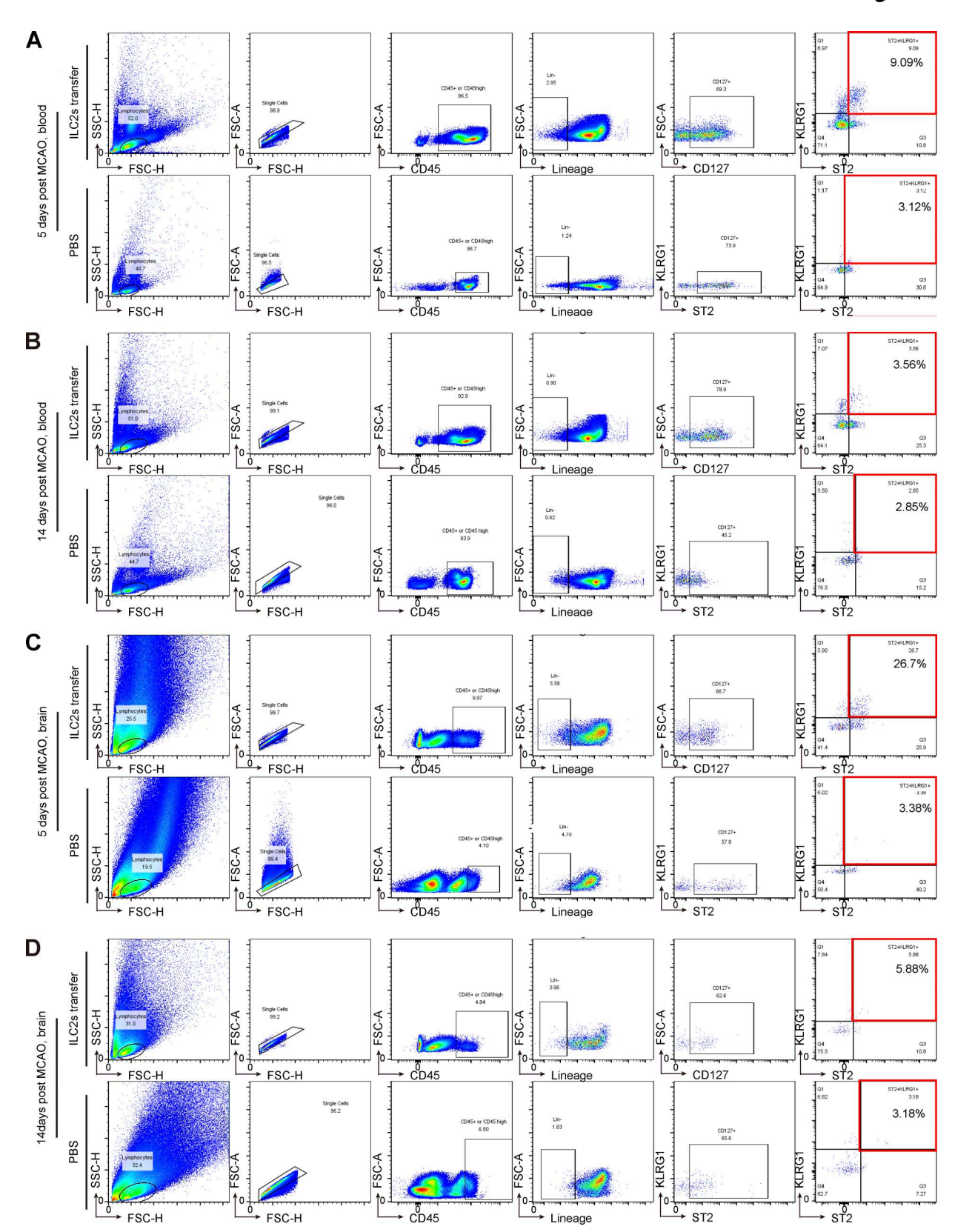


Figure S2. **Gating strategy and results of FACS and flow cytometry after MCAO and ILC2 injection. (A)** Flow cytometry gating strategies and results for blood ILC2s (Lin-CD45+CD127+ST2+KLRG1+) at day 5 after MCAO in the ILC2-transferred group (upper row) and the control group (lower row). **(B)** Flow cytometry gating strategies and results for blood ILC2s at day 14 after MCAO in the ILC2-transferred group (upper row) and the control group (lower row). **(C)** Flow cytometry gating strategies and results for brain ILC2s (Lin-CD45high CD127+ST2+KLRG1+) at day 5 after MCAO in the ILC2-transferred group (upper row) and the control group (lower row). **(D)** Flow cytometry gating strategies and results for brain ILC2 (Lin-CD45+ST2+KLRG1+) at day 14 after MCAO in the ILC2-transferred group (upper row) and the control group (lower row).



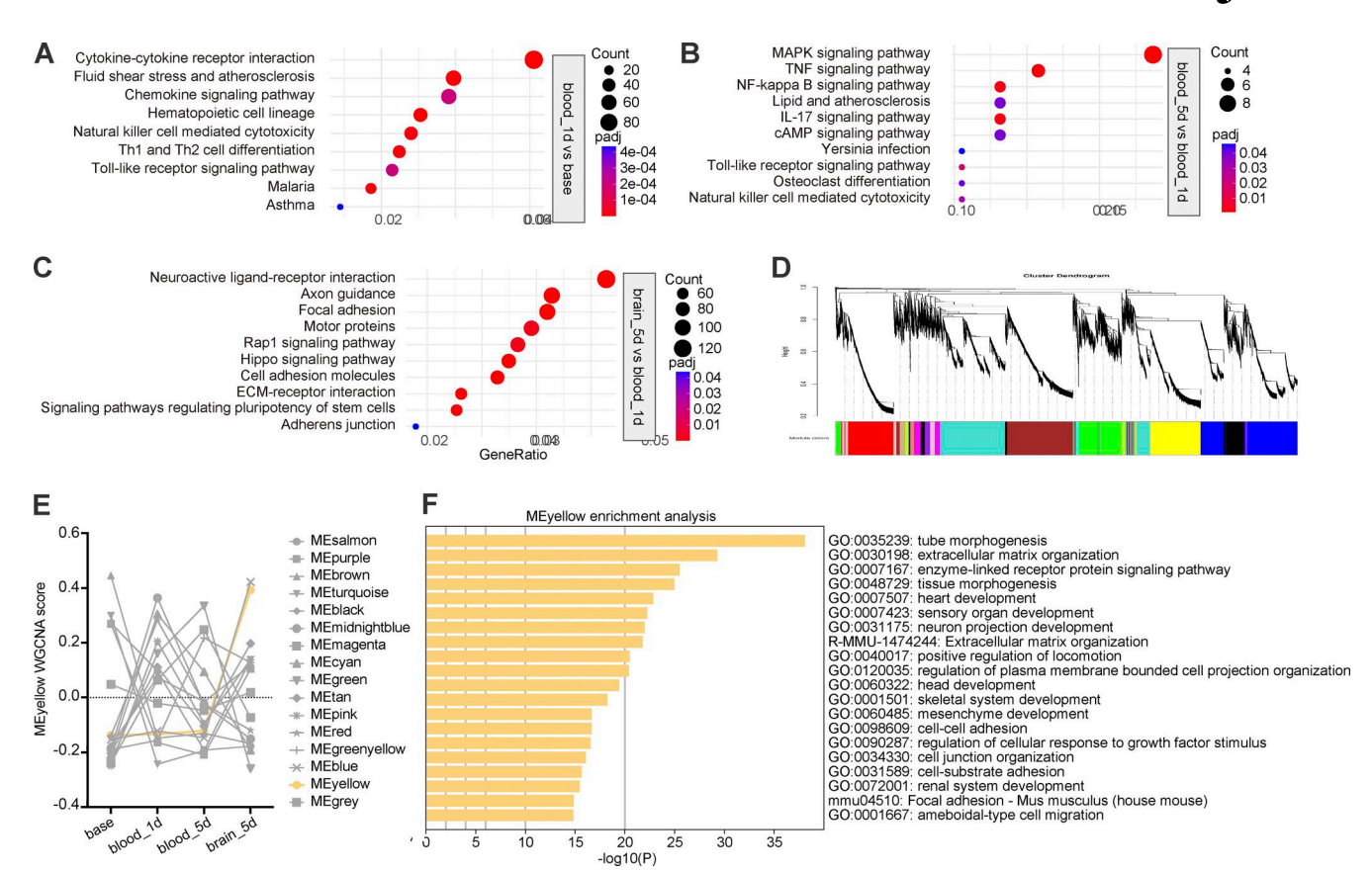


Figure S3. **SMART-seq of transferred ILC2s. (A–C)** KEGG enrichment pathways of DEGs between blood_1d versus baseline, blood_5d versus blood_1d, and brain_5d versus blood_5d. **(D)** WGCNA Dynamic Tree Cut. **(E)** Group-averaged WGCNA modular scores, among which MEyellow is the only upregulating module between four groups (brain_5d > blood_5d > blood_1d > base). **(F)** GO-enrichment results of all 1,716 MEyellow genes. KEGG, Kyoto Encyclopedia of Genes and Genomes.



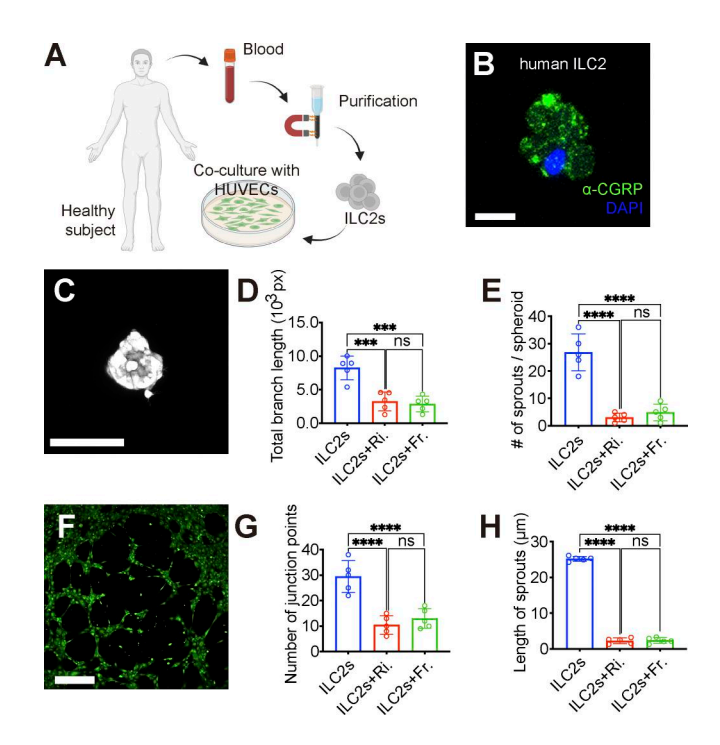


Figure S4. The pro-angiogenic effect of human-derived ILC2s can be inhibited by α-CGRP antibody or CGRP receptor antibody. (A) In vitro co-culture experiment of human-derived ILC2s and HUVECs (created with https://BioRender.com). (B) Human-derived ILC2s expressing α-CGRP. (C-E) Human-derived cell assay: In vitro HUVEC sprouting experiment, quantification of the number and length of sprouts per spheroid (n = 5). Scale bar, 100 μm. Data are shown as bar plots (SD, median), analyzed by one-way ANOVA with Tukey's multiple comparisons. In C, ILC2s versus ILC2s+Ri.: ***P = 0.0002. ILC2s vs ILC2s+Fr.: ****P = 0.0005. ILC2s+Ri. vs ILC2s+Fr.: P > 0.05. In D, ****P < 0.0001, ns indicates P > 0.05. (F-H) Human-derived cell assay: In vitro HUVEC tube formation experiment, quantification of node number and branch length of tubular structures (n = 5). Ri, rimegepant; Fr, fremanezumab. Scale bar, 250 μm. Data are shown as bar plots (SD, median), analyzed by one-way ANOVA with Tukey's multiple comparisons. ****P < 0.0001, ns indicates P > 0.05.

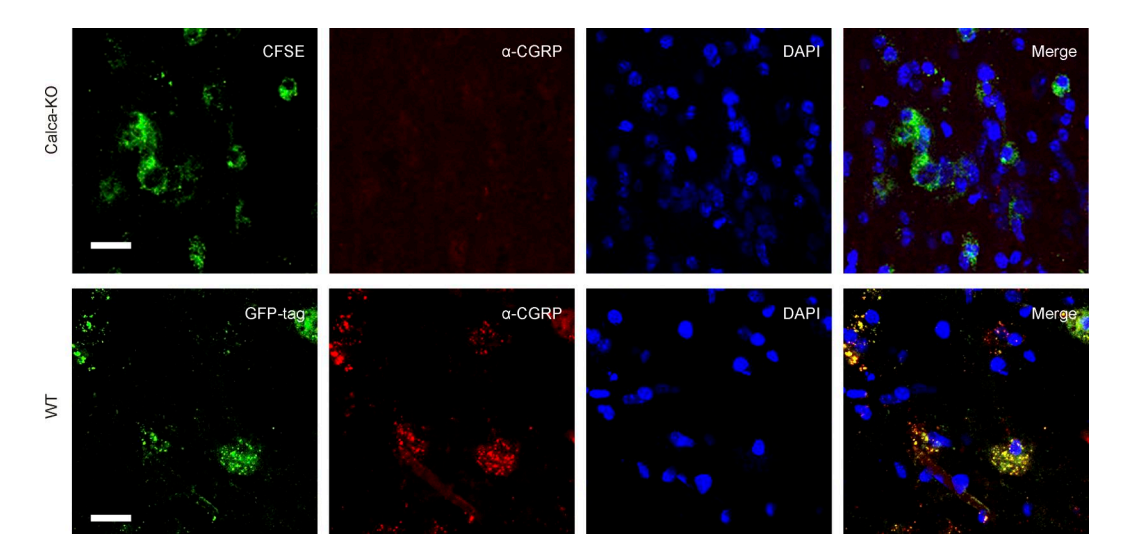


Figure S5. Immunofluorescent staining shows the colocalization and expression of α -CGRP with infused ILC2s. Representative α -CGRP (red), CFSE/GFP-tag (green, CFSE for Calca-KO ILC2s, GFP-tag for WT ILC2s), DAPI (blue), and merged images were captured with confocal fluorescent microscopy. Scale bars, 20 μ m.